Characterization of gap-discontinuities in microstrip structures, used for opto-electronic microwave switching

Slotboom, B.M.

Award date:
1992

AFDELING DER ELEKTROTECHNIEK
TECHNISCHE UNIVERSITEIT EINDHOVEN
VAKGROEP TELECOMMUNICATIE, EC

Characterization of Gap-Discontinuities in Microstrip Structures, Used for Opto-Electronic Microwave Switching

by Bas M. Slotboom

Verslag van het afstudeerwerk
uitgevoerd van december 1991 tot augustus 1992
Afstudeerhoogleraar: Prof. Dr. ir. G. Brussaard
Begeleiders: Prof. Dr. ir. G. Brussaard
Dr. S. Tedjini

SUMMARY

Optoelectronic switching of passive devices offers a lot of advantages over electronic switching. Ultrafast and jitter-free response are the most obvious advantages in applications that require high-speed switching and high resolution.

An optoelectronic transmission line switch is basically a gap discontinuity in a microstrip or coplanar waveguide structure on a semi-insulating substrate. If the gap is illuminated, free electron-hole pairs are generated in the gap. This makes the gap conductive, and "closes" the switch. This is called the photoconductive effect. Because optoelectronic switches must have good electrical as well as optical characteristics, GaAs is often used as the switching material.

At the Laboratoire d'Electromagnétisme, Micro-ondes et Opto-électronique (LEMO) of the Institut National Polytechnique de Grenoble (INPG) where this graduation work is performed, optoelectronic microwave switches on GaAs substrate doped with chromium (Cr) were realized. The Cr doping decreases the carrier lifetime, and thus increases the switching speed.

To examine the behaviour of the switch in the "off"-state (without illumination), microstrip and coplanar waveguide devices were fabricated on Epsilam-10 substrates. To perform measurements these non-coaxial devices have to be mounted into fixtures. Some characteristics of the devices (e.g. the characteristic impedance) are measured in the time-domain with the TDR technique. For a total characterization of these non-coaxial devices, high-frequency measurements have to be performed. At high frequencies micowave devices are characterized by their scatter-parameters. It is difficult to measure the S-parameters of the Device Under Test (DUT) directly, because the DUT is mounted into a fixture. Extracting the DUT characteristics from the overall measured characteristics can be done with different so-called de-embedding methods.

The one-tier de-embedding TRL-Calibration method was investigated. Results were compared with results obtained when a normal coaxial calibration is used, and with simulations done with the simulation and analysis software-package SuperCompact. The advantages of the TRL method are more stable measurement results and a greatly reduced influence of the fixture on the measurements. However, at high frequencies (10 GHz) the implementation of the calibration is very delicate.

Despite a lot of problems with the realization of the Cr:GaAs devices, some measurements could be performed. The measurements show a clear influence of the bonding wires that are used in the fixtures of these devices, on the results.

TABLE OF CONTENTS

LIST OF ABBREVIATIONS

CIME	Centre Universitaire du Micro-Electronique.
CPW	coplanar waveguide.
CW	continuous wave.
DC	direct current.
DUT	device under test.
ECL	Ecole Centrale de Lyon.
GHz	giga herz (10^9 Herz).
IMPATT	impact ionization avalanche transit time.
INPG	Institut National Polytechnique de Grenoble.
LEMO	Laboratoire Electromagnetisme Micro-onde et Optoelectronique.
LHOG	Laboratoire d'Hyperfréquence et d'Optiques Guidée.
MESFET	metal-semiconductor field effect transistor.
MIC	microwave integrated circuits.
MMIC	monolithic microwave integrated circuits.
MS	microstrip.
NA	network analyzer.
RF	radio frequency.
SWR	standing wave ratio.
TDR	time domain reflectometry.
TEM	transversale electromagnetic.
THz	terra herz (10^{12} Herz).
TRL	through-reflect-line.
TSD	through-short-delay.
VNA	vectorial network analyzer.

CHAPTER 0

INTRODUCTION

From December 1991 to July 1992 I performed the graduation work for my Master Thesis at the Laboratoire d'Electromagnétisme, Micro-ondes et Opto-électronique (LEMO) of the Institut National Polytechnique de Grenoble (INPG) in France. In 1989 the group "Opto-Microonde" at LEMO of Dr.S.Tedjini started a research project in the quite new and promising field of optoelectronic switching of passive elements. The aim of the project can be summarized as: *"to realize, characterize and simulate high performance photoconductive transmission line switches, integrated in microstrip and coplanar waveguide structures on Cr:GaAs substrates"*. From December 1991 until July 1992 I worked together with S.Sani (Eng.) on this project. Mr.Sani is doing a PhD. Thesis on this subject and will finish in December 1992.

In the past few years tremendous advances have been made in both microwave and optical technology. This gave the possibility of optically controlling microwave devices by using the photoconductivity-effect. For example optical control of several active microwave devices like IMPATT, TRAPATT, GaAs MESFET, HEMT and transferred-electron devices have been described by several authors ([2],[6]). Optical control of microwave devices offers a lot of advantages, like:

1) near perfect isolation between the controlling and the controlled device.
2) immunity from electromagnetic interference.
3) light weight and compact size.
4) extremely fast response.
5) high power handling capability
6) possibilities for monolithic integration

Applications of optically controlling microwave signals are not only realized with active devices. A lot of control applications, using optical pulses, are based on the optoelectronic switching of passive elements. The transmission line switch is the most wellknown example of a passive switch. It makes switching speeds in the order of picoseconds possible. The transmission line switch can be used in several applications, like high resolution radar systems, high speed digital (communication) systems and on-wafer measurements of monolithic microwave integrated circuits (MMICs).

The transmission line switch is in its most simple form a gap-discontinuity in the central strip of a microstrip or coplanar waveguide structure, see Figure 0.1.

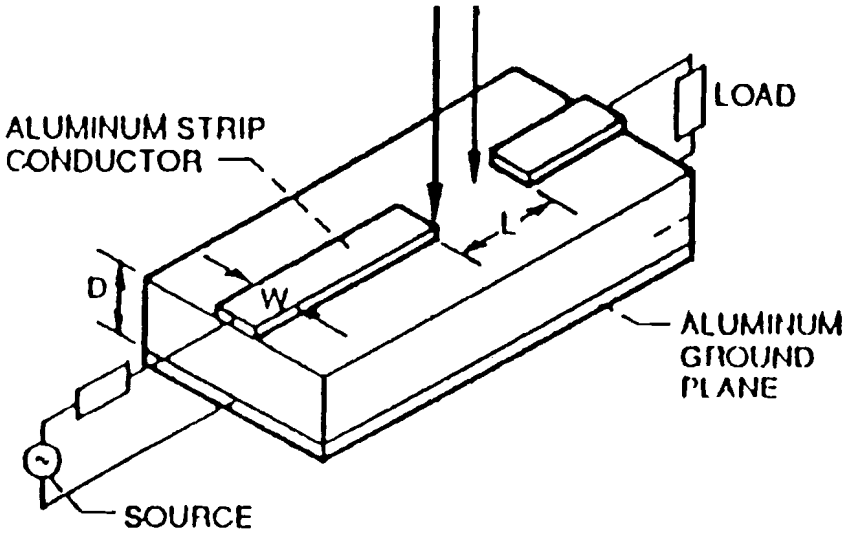

Figure 0.1: The Optoelectronic Microwave Switch

When the gap is illuminated, free electron-hole pairs are generated and the gap becomes conductive, which "closes" the switch. This is called the photoconductive effect. To investigate microwave switches I made several microstrip and coplanar waveguide devices: with and without gap-discontinuities, with various transmission line lengths, mounted into different types of fixtures and on different kinds of substrates. To perform measurements with these high speed devices different high frequency measurement methods are developed the last decade. The measurements in the frequency domain are done with a Vectorial Network Analyzer (VNA). At LEMO we used the HP 8510 B Vectorial Network Analyzer. Figure 0.2 shows a photograph of the measurement setup.

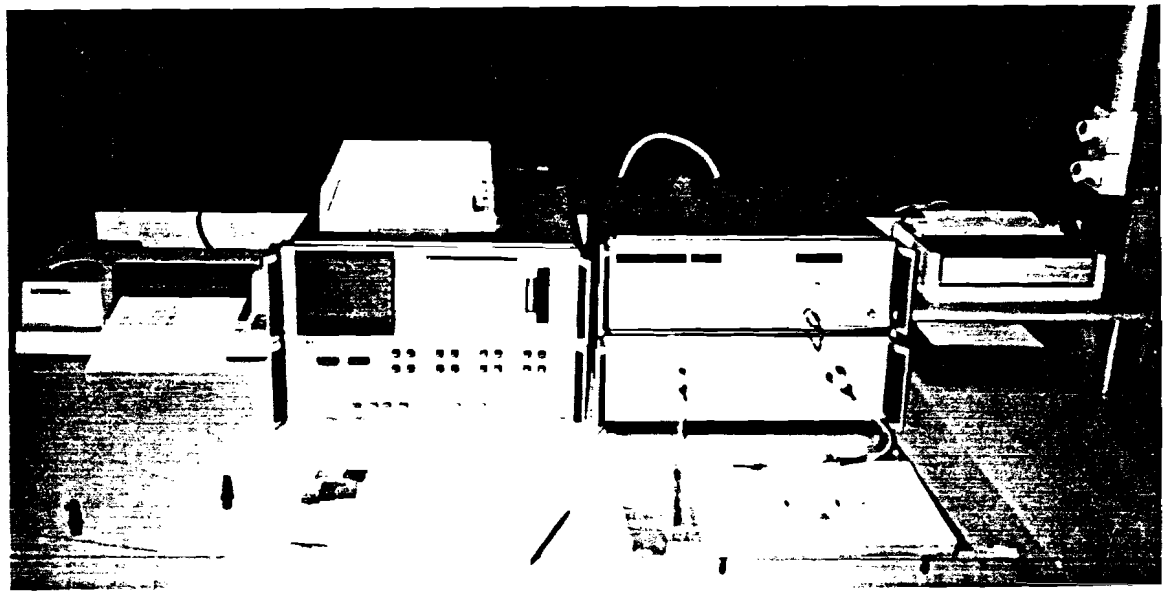

Figure 0.2: HP 8510 B Measurement Setup at LHOG.

We fabricated optoelectronic microwave switches on Cr:GaAs substrates. The Cr:GaAs material has the best qualifications (electrical and optical) for excellent optoelectronic switching performance.

Because the fabrication of the devices on Cr:GaAs had a lot of delay, transmission lines with and without gap-discontinuities are fabricated on a substrate called Epsilam-10. Epsilam-10 has a high relative permittivity just like Cr:GaAs and can therefore be used very well as a substitution for Cr:GaAs in "off"-state microwave switch measurements. With these Epsilam-10 devices the implementation and the validity at high frequencies of different measurement methods are examined.

The devices on Cr:GaAs were ready in July 1992. The preliminary measurement results which I obtained with these devices are described in paragraph 4.3, Chapter 4. They are compared with the earlier obtained frequency measurements of the Epsilam-10 devices.

All the realized devices on the Cr:GaAs and on the Epsilam-10 substrates, used in the experiments, are made in microstrip and coplanar waveguide structures. In Appendix A the microstrip and coplanar waveguide transmission media are described and discussed in general.

In the next chapter I will introduce optoelectronic microwave switching: the principle, the recent developments and some applications.

CHAPTER 1

OPTOELECTRONIC MICROWAVE SWITCHING

1.1 OPTOELECTRONIC SWITCHING METHODS

Optoelectronic microwave switching is a technique that allows optically controlled abrupt changes of amplitude of a microwave signal via photo-induced electron-hole pairs. These excess carriers are generated within the semiconductor region of a special high speed switching element: The Optoelectronic Switch.

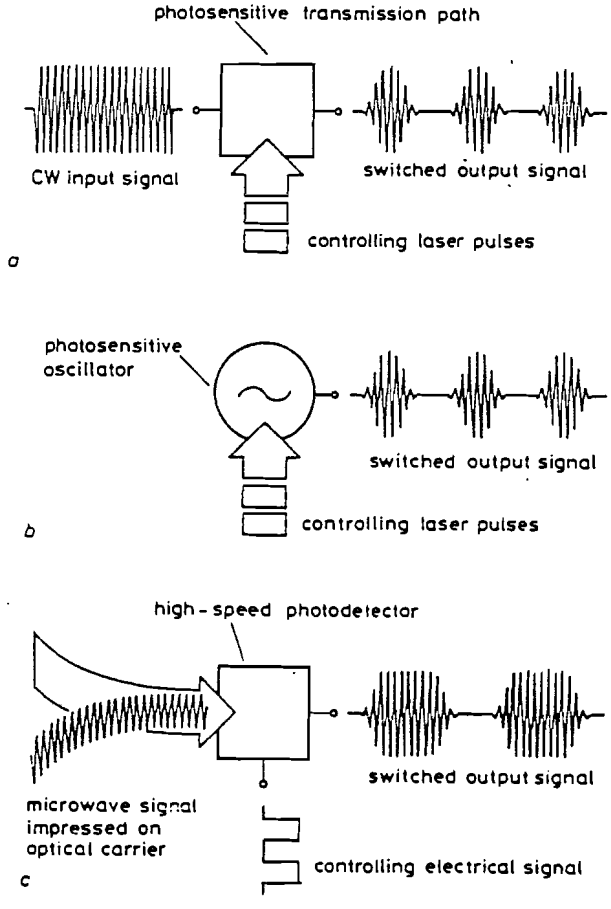

Figure 1.1: Basic principles of optoelectronic microwave switching:
a transmission line switching
b oscillator switching
c detector switching

Figure 1.1 illustrates three basic methods of microwave switching [1]. The most commonly used method is the transmission line switching (Fig. 1.1a). Here a two port switching device is fed by a continuous microwave signal. Switching is achieved by focusing the controlling laser pulses on a photosensitive path in the switch. This is the switching principle on which the project at LEMO is based.
Figure 1.1b shows the principle of oscillator switching. The oscillations of a solid-state microwave source are excited, enhanced or quenched by the controlling laser pulses.
The detector switching, as described in Figure 1.1c, is a totally different technique. It is a hybrid of electronic and optical switching. A Radio Frequency (RF) signal is impressed on an optical carrier (the laser beam from a laser-diode), and supplied to a photodiode (the detector). Switching is achieved by reverse biasing the

detector in the "on"-state (optically sensitive), and forward biasing in the "off"-state (optically insensitive). Thus switching of a microwave signal impressed on an optical carrier is achieved by the bias-controlled photoconductivity of a high speed photodetector.

1.2 MODES OF OPERATION

The physical mechanism used in optoelectronic microwave switching is the generation of free carriers within the illuminated semiconductor region. This happens when light with a photon energy greater than or equal to the semiconductor bandgap is absorbed. As a result of the optically controlled carrier generation, the electrical properties of the plasma region are changed, which makes switching possible.
Apart from this, the switching process also depends on the structure of the excited region. This is why the switch can be operated in a photoconductive mode or a dielectric mode.

1.2.1 The Dielectric Mode

In the dielectric mode the effect used is that the photo-induced plasma causes a change in the refractive index, for high frequency signals [2]. Figure 1.2 shows the interaction of a Radio Frequency (RF) signal with an electron-hole plasma in a semiconductor.

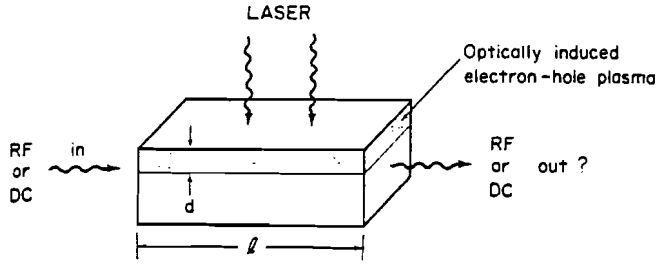

Figure 1.2: Interaction of lowfrequency electromagnetic waves with the photo-induced electron-hole plasma in a semiconductor: d is the penetration depth of the optical beam.

The electron-hole plasma in the layer, with thickness d, introduces the following complex permittivity in the plasma region.

$$\epsilon_r = \epsilon_r' - j\epsilon_r'' = \epsilon_L - \frac{\omega_p^2}{\omega^2+\nu^2} - \frac{j\nu}{\omega} * \frac{\omega_p^2}{\omega^2+\nu^2} \qquad (1.1)$$

ω : angular frequency of the RF field.
ϵ_L: dielectric constant host lattice.
v : carrier collision frequency.
ω_p: plasma frequency.

$$\omega_p = \frac{ne^2}{\epsilon_0 m^*} \tag{1.2}$$

n : density of the photo-induced excess carriers, proportional to the laser intensity.
e : electronic charge.
m^*: effective mass.
ϵ_0: permittivity of vacuum.

For low frequency signals, $\omega << v$ and $\omega_p << v$, the photo-induced carrier density will not affect the real part of ϵ_r. However for high frequency RF-signals (30-100 GHz) the effect of the photo-induced carrier density on the real part of ϵ_r can not be neglected. For high frequency RF-signals the photo-induced plasma will cause refractive index change for the RF-signal, effectively making also phase modulation on the RF-signal. A disadvantage of this mode is that it needs extremely high excess carrier densities, as can be seen from equation 1.2.

1.2.2 The Photoconductive mode

In the photoconductive mode the wavelenghts of the RF-signals to be controlled are normally much greater than the physical dimensions of the plasma region. It is the most simple, but also the most promising and most widely used control mechanism for optoelectronic microwave switching. The principle of operation will be explained in the next paragraph.

1.3 PHOTOCONDUCTIVE TRANSMISSION LINE SWITCHING

1.3.1 The principle of operation

The principle of operation will be explained by a high-speed optoelectronic microwave switch on a silicon substrate, as it was first presented by Auston in 1975 [3].

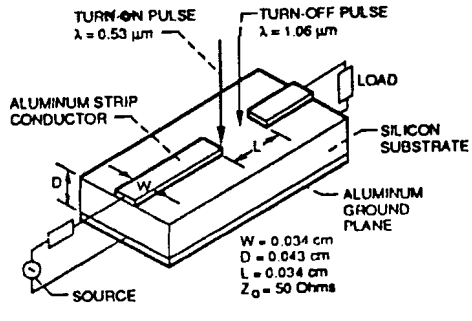

Figure 1.3: Optoelectronic Microwave Switch

The switch, schematically shown in Figure 1.3, consists of a 50 Ω microstrip transmission line structure fabricated on a high-resistivity silicon substrate. In the top strip conductor a gap of length L is etched. Input and output microwave signals are coupled to the silicon by 3-mm coax-to-microstrip launchers. When the gap is illuminated, absorption of the photons take place in the silicon substrate. The absorbed photons cause electron transfer from the bound state to the free state, thereby creating free electron-hole pairs.

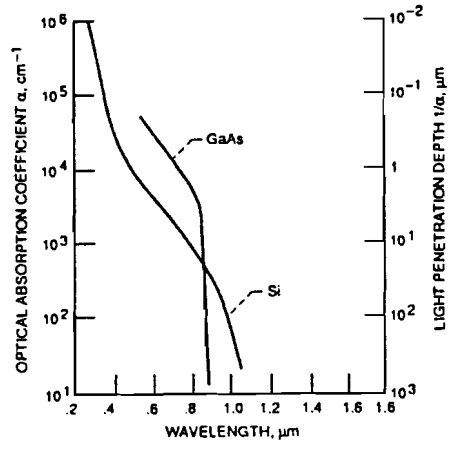

Figure 1.4: Optical absorption coefficient for silicon and GaAs as a function of the wavelength.

In Figure 1.4 the optical absorption coefficient (α) for silicon is shown as a function of the incident illumination wavelength. This figure shows that if the gap of the microstrip is illuminated by an optical pulse with a sufficiently high intensity and a wavelength less than 0.55 μm, the switch can be turned on. Because in this wavelength range the absorption coefficient is very large, and hence the absorption depth ($1/\alpha$) is very small, a thin surface plasma is formed. This surface plasma closes the gap producing a net resistance which is much less than the characteristic impedance of the microstrip line, thus permitting efficient transmission across the device.
A second optical pulse with a wavelength greater than 1μm can turn the switch off.
The large absorption depth, corresponding to the small absorption coefficient, gives rise to volume photoconductivity. This volume photoconductivity short circuits the top strip conductor to the bottom ground plane of the microstrip. The short circuit reflects the incident signal back to the generator resulting in a negligible forward transmission.

In experimental switches, on silicon substrates, one chooses for the wavelengths to switch "on" and "off" respectively 0.53 μm and 1.06 μm, because they can be easily generated using a Nd:glass laser.

The simplified equivalent circuits of the switch in the "on" and "off"-state are given in Figure 1.5. For the conductances G_1 and G_2 can be written:

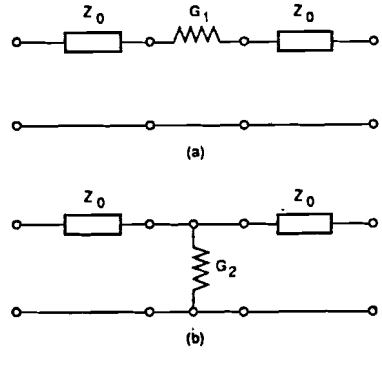

$$G_1 = \frac{4n_r}{(n_r+1)^2} * \frac{e}{h\nu} * (\mu_n+\mu_p) * \frac{E_1}{L^2} \quad (1.3)$$

$$G_2 = \frac{2\alpha_2}{D} * \frac{e}{h\nu} * (\mu_n+\mu_p) * E_2 \quad (1.4)$$

Figure 1.5: Equivalent circuit of the switch: a) on-state b) off-state

n_r: refractive index substrate.
hv/e: photon energy in volts.
$\mu_n+\mu_p$: sum of the electron and hole mobilities.

E_1: energy of the turn-on optical pulse.
E_2: energy of the turn-off optical pulse.
α_2: absorption coefficient at the turn-off wavelength.
D: substrate thickness.

G_1 is in the order of 5 mhos (R_1 = 0.2 Ω) which is a very small impedance compared to the 50 Ω microstrip characteristic impedance, and hence a good approximation of a series short circuit.
G_2 is in the order of 5.6 mhos which is very large compared to the 0.02 mhos characteristic of the microstrip, and thus a good approximation of a shunt short circuit.

1.3.2 Switching Speed & Repetition Rate

By giving the following general equations for the plasma photoconductivity, $\Delta\sigma$, generated by the laserlight some characteristics of the optical switch can be derived.

$$\Delta\sigma(d) = \Delta\sigma_s \exp(-\alpha d) \tag{1.5}$$

d: depth variable, d=0 at the surface, d=D at the ground plate (Figure 1.3).
$\Delta\sigma_s$: surface conductivity at d=0.

$$\Delta\sigma_S = \frac{q}{hc} * (\mu_n+\mu_p) * (1-R) * S\alpha * \lambda_0\gamma\frac{W}{A} \tag{1.6}$$

$$W = P * t_w \tag{1.7}$$

μ_n,μ_p: effective mobilities of electrons and holes.
R: surface reflectivity.
S: relative spectral response of the semiconductor material exhibiting a peak response at λ_0.
α: absorption coefficient.
γ: parameter that covers the relative loss of carriers during the excitation phase: $0 \le \gamma \le 1$.
A: illuminated area.
W: optical pulse energy.
P: radiant peak power.
t_w: laser pulse width.

From equation 1.5 it can be seen that a large absorption coefficient α results in a small absorption depth, as described before. Now two different cases can be distinguished.

In the case of slow-recombination material, the excess carrier lifetime is much greater than the laser pulse width, $\tau >> t_w$. Optical switches with slow-recombination substrates, like silicon, need a turn-off pulse. After putting the switch in the "off"- state the optically generated electrons and holes still remain. The turn-off pulse has just anulled the effect of the surface layer of photoconductivity. Consequently the switching speed can be extremely fast. The most important limitations are the duration and the amplitude of the optical pulses.

However the repetition rate of the switch depends on the recombination time, or lifetime, of the excess carriers. Since the recombination time is "long" (in the order of 1 μs for silicon) the switch has a slow repetition rate.

By doping the silicon with gold atoms, or by using Cr doped GaAs as a substrate, the carrier life time is decreased. In this second case the excess carrier lifetime is much smaller than the laser pulse width, $\tau << t_w$. The carrier recombination diminishes the optically generated carriers instantaneously. This implies that only a turn-on pulse is needed. Optical switches with these ultra-fast substrate materials turn off automatically. In this way picosecond switching with high repetition rates, up to 1 GHz, is possible.

However, since there is already carrier recombination during the excitation phase, a considerable loss of excess carriers, indicated by $\gamma < 1$, must be accepted. This strongly reduces the switching efficiency (see equation 1.6). This indicates that there is a trade-off between high speed and high repetition rates on one side and switching efficiency on the other side. So the doping concentration can not be too high.

1.4 PICOSECOND OPTOELECTRONIC SWITCHING

The first picosecond optoelectronic GaAs switch was presented by Lee in 1977 [5]. The structure of the switch used by Lee is shown in Figure 1.6. In this configuration a high-strength dielectric is used as an insulator, instead of the semiconductor switching material (see for example Figure 1.3).

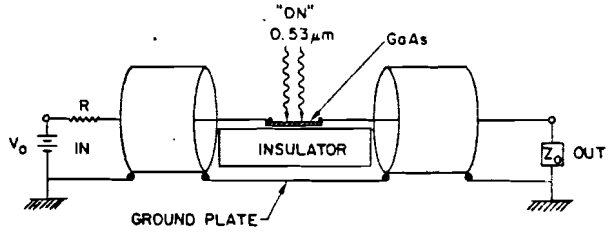

Figure 1.6: The structure of the picosecond opto-electronic switch, with a slab of GaAs as the switching element.

Because the size of the switch is not any more restricted by the thickness of the substrate the power handling capability of the device is increased. The GaAs substrate is doped with Cr atoms, to produce deep level recombination centers. This results in a faster recombination of the electrons. Thus, the lifetime of the excess carriers is decreased.

In order to have a good isolation between the input and the output, the photoconductive substrate materials must have a high dark resistivity.

Semiconductor	Eg (ev)	Carrier Lifetime (ns)	Dark Resistivity (Ω-cm)
Si (intrinsic)	1.16	10^4	5×10^4
SoS		10 ~ 1 ps	
*Cr:GaAs	1.42	< 1	$>10^7$
Fe:InP	1.29	< 1	$>10^7$
*CdS_xSe_{1-x}	1.8 ~ 2.4	> 10	$> 10^7$
GaP	2.24	> 1	$> 10^7$
*(Diamond (IIa))	5.5	< 1	$> 10^{16}$
Fe:In:GaAs		500 ~ 100 ps	
GaAs on SoS		20 ps	

*First developed at the University of Maryland

Table 1.1: Semiconductor materials investigated for high speed, high power photoconductive switching.

Table 1.1 shows some specific figures of several picosecond photoconductors. The high dark resistivity of the switch makes it non-conductive in the dark "off"-state. Picosecond optical pulses illuminating the photoconductor close the switch instanteneously. The rise time of the electrical pulse will approach that of the laser pulse. The actual shape of the electrical pulse depends on the time the switch remains closed: the photoconductive lifetime. The photoconductive lifetime, τ, depends on the carrier recombination time.
If $\tau >> 2L/v$, the roundtrip propagation time, then a square waveform appears at the load with rise and fall times equal to rise and fall time of the laser pulse. Here L is the length of the charged line, and v is the velocity of the voltage wave propagating on the line. If $\tau << 2L/v$, a single sided exponential waveform appears on the line, with a fall time equal to the photoconductive decay time.

The maximum output voltage is:

$$V_{out} = V_c * \frac{Z_0}{(2Z_0+R_s)} \tag{1.8}$$

With R_s, the dynamic resistance under laser illumination given by:

$$R_s(t) = R_c + \frac{l_{gap}^2}{(e\mu N(t))} \tag{1.9}$$

N(t): Number of photo-induced charge carriers (proportional to the optical energy of the pulse.
l: gaplength.
R_c: specific contact resistance for ohmic contacts.

1.4.1 Applications

* The High Power Switch

For this application one usually requires the switch to transfer energy efficiently to the load. Therefore $R_s << Z_0$ is wanted (see equation 1.8). However at the same time one requires a large gaplength, because the voltage across the gap must be very high for high power applications. The maximum voltage across the gap is:

$$V_{max} = l_{gap} * E_{br} \tag{1.10}$$

E_{br}: intrinsic breakdown field (in the order of $2 \cdot 10^5$ V/cm)

These conditions and the equations (1.8), (1.9) and (1.10) make clear that a high N(t) i.e. a high optical energy is needed for high power switching.
High power switches with a size of some millimeters or even centimeters and a high maximum voltage of 100 kV are possible.

* High speed optical detector and optical electronic sampler

In these applications the high speed is the most important feature. Therefore the efficiency of the energy transfer can be sacrificed a bit. To maintain a linear relationship between V_{out} and the laser intensity, one needs $R_s(t) >> Z_0$ (see equation 1.8 and 1.9). Since the output voltage requirement is low one chooses a small gap, in the order of micrometers.

Optoelectronic microwave switching is applied in:

* High-speed digital communication networks.
* High-resolution radar systems.
* Satellite-borne switching concepts [1].

A lot of practical applications make use of the generation of micro-and millimeter-waves by picosecond photoconductors. The following practical applications can be mentioned:

* On-wafer measurement of monolithically integrated millimeter-wave or high speed digital circuits.

* Generation of pulsed or CW microwaves via direct dc to RF conversion using picosecond photoconductive switches. By using "a frozen wave" generator microwaves with a small number of cycles can be generated. Microwaves with a large number of cycles can be generated by the impulse excitation of a resonant microwave cavity [2].

* Picosecond photoconducting dipole antenna's. These antenna's, when illuminated with femtosecond optical pulses, radiate electrical pulses with frequency spectra extending from dc-to-THz.[7]

1.5 COMPARISON OF OPTICAL AND ELECTRONIC SWITCHES

Optical switches give the opportunity to switch very fast, in the order of picoseconds. They can also handle moderately high powers, unlike "normal" electronic switches that use GaAs MESFET's or PIN diodes. The power these electronic switches can handle is limited by the breakdown voltage and thermal dissipation.

One of the most important characteristics of the photoconductive switch is jitter-free response. This is possible because the controlling optical signal and the gated microwave signal are totally electrically isolated. Jitter-free response allows perfect time synchronization between the generated electric signals and the optical pulses.

MESFET and PIN diode electronic switches require special low-capacitance bias circuits with charging time significantly smaller than the switching time. However, optoelectronic switches do not require any bias circuit.

The electronic switches have to be integrated in the substrate, whereas optoelectronic switches are very simple to construct as a result of their planar topology. Because optical sources, detectors and transistors all have planar topology, they can all be laid out and interconnected by planar transmission lines.

Because of these advantages of optical passive microwave switches over regular electronic switches, and their simplicity of operation, a lot of research is being done in this quite new field of optoelectronic technology.

CHAPTER 2

MICROWAVE DEVICE ANALYSIS.

2.1 INTRODUCTION

The gap-devices, and the other microstrip and coplanar waveguide transmission line components, which we realized, can be represented by a basic two port network (see Figure 2.1).

In normal network analysis the two port network can be described by a number of parameter sets. The Y-, Z- and H-parameter sets are the most wellknown. They relate total voltages and total currents at each of the two ports. The only difference between the parameter sets is the choice of the independent and dependent parameters.

Figure 2.1: Two port device representation

Y-parameters: $I_1 = y_{11}V_1 + y_{12}V_2$
$I_2 = y_{21}V_1 + y_{22}V_2$

Z-parameters: $V_1 = z_{11}I_1 + z_{12}I_2$
$V_2 = z_{21}I_1 + z_{22}I_2$

H-parameters: $V_1 = h_{11}I_1 + h_{12}V_2$
$I_2 = h_{21}I_1 + h_{22}V_2$

To determine for example z_{11} by measurement, one sets $I_2=0$ by leaving port 2 open:

$$z_{11} = \frac{V_1}{I_1}\Big|_{(I_2=0)} \qquad y_{22} = \frac{I_2}{V_2}\Big|_{(V_1=0)} \qquad h_{12} = \frac{V_1}{V_2}\Big|_{(I_1=0)} \tag{2.1}$$

Determining y_{22} can be done in the same manner by shortening port 1, and h_{12} (the reverse voltage gain) is measured as the ratio of V_1 to V_2 with the input port open circuited. We note here that it is necessary to have open and short circuits to make these measurements possible.

At higher frequencies this gives the following problems:

1) There is no equipment available that can measure total voltages and total currents at the ports of the network.
2) Short circuits and open circuits are difficult to achieve over a broad band of frequencies.

To overcome these problems another method of characterization is used in high frequency cases. Instead of total voltages and total currents, the logical variables used at high frequencies are travelling waves of voltage, current and power.

2.2 TRANSMISSION LINES

At microwave frequencies, voltage, current and power are considered to be in the form of travelling waves, travelling in both directions along the transmission line. If there are no discontinuities on the line it is called a uniform transmission line. It can be thought of as an equivalent series impedance ($R+j\omega L$) and an equivalent shunt admittance ($G+j\omega C$) per unit length, as is shown in Figure 2.2.
The parameters R,L,C and G are the primary transmission line parameters.

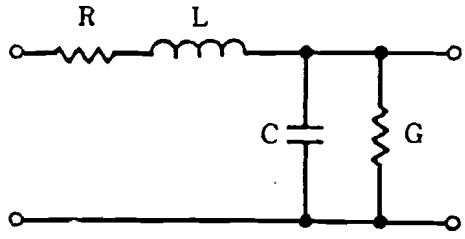

Figure 2.2: Uniform transmission line representation

A transmission line can also be characterized by its characteristic impedance Z_c and its propagation parameter γ. These are the secondary transmission line parameters. The impedance Z_c is the ratio between the total voltage and the total current at any point along the line: V_t/I_t.
The total voltage and total current can be described as a function of travelling voltage waves in two directions along the line.

$$V_t = E_i e^{-\gamma x} + E_r e^{\gamma x}$$
$$I_t = \frac{E_i}{Z_c} e^{-\gamma x} - \frac{E_r}{Z_c} e^{\gamma x} \qquad (2.2)$$

$E_i \exp(-\gamma x)$: incident voltage wave.
$E_r \exp(\gamma x)$: reflected voltage wave.

The propagation parameter is given as:

$$\gamma = \alpha + j\beta \tag{2.3}$$

α: loss constant.
ß: propagation constant or wave constant.

The secondary parameters can be expressed as a function of the primary parameters, as:

$$Z_c = \sqrt{\frac{R + j\omega L}{G + j\omega C}} \qquad \gamma = \sqrt{(R + j\omega L)(G + j\omega C)} \tag{2.4}$$

A lossless line would simply have a series inductance and a shunt capacitance, so:

$$Z_c = \sqrt{\frac{L}{C}} \quad , \qquad \gamma = j\omega\sqrt{LC} \tag{2.5}$$

Another very useful relationship is the Reflection Coefficient: Γ. It gives an indication about the quality of the impedance match between the load impedance and the characteristic line impedance.

$$\Gamma = \frac{E_r}{E_i} = \frac{Z_L - Z_c}{Z_L + Z_c} = |\Gamma|\, e^{j\theta_\Gamma} \quad , \qquad |\Gamma| = \rho \tag{2.6}$$

The Standing Wave Ratio (SWR) is defined as the ratio between the maximum and minimum voltage or electric field along the line.

$$SWR = \frac{1 + \rho}{1 - \rho} \tag{2.7}$$

2.3 SCATTERING PARAMETERS

If we now insert a two port network into the transmission line, we are having four travelling voltage waves that are interrelated.

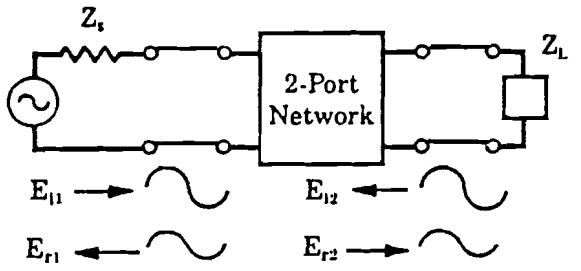

Figure 2.3: Two port network with traveling waves

These four travelling voltage waves can be related by combining the expressions for total voltages and total current and the H-parameter set. The equations can now be rearranged such that the incident voltage waves are the independent variables and the reflected voltage waves are the dependent variables:

$$E_{r1} = f_{11}E_{i1} + f_{12}E_{i2}$$

$$E_{r2} = f_{21}E_{i1} + f_{22}E_{i2} \qquad (2.8)$$

Since the F-parameters relate those waves who are scattered (or reflected) from the two port to those waves incident upon the two port, this new parameter set is called the scattering-parameter set. If we go a bit further and divide the equations by $\sqrt{(Z_c)}$ the relationship does not change, but the variables do. The new variables are now:

$$a_x = \frac{E_{ix}}{\sqrt{Z_c}}, \qquad b_x = \frac{E_{rx}}{\sqrt{Z_c}} \qquad (2.9)$$

Notice that $[a_1]^2$, $[b_1]^2$, $[a_2]^2$, and $[b_2]^2$ have the dimension of power now.

$[a_1]^2$ represents the incident power on port 1
$[b_1]^2$ represents the reflected power from port 1

In a lossless two port network we should have:

incident power ≡ reflected power: $[a_1]^2+[a_2]^2 = [b_1]^2+[b_2]^2$

These new variables, which represent in fact normalized field strengths, can be related by the S-parameters:

$$b_1 = S_{11}a_1 + S_{12}a_2$$
$$b_2 = S_{21}a_1 + S_{22}a_2 \qquad (2.10)$$

The S-parameters can be measured by terminating the output port with an impedance equal to the characteristic impedance of the transmission line. So:

$$S_{11} = \frac{b_1}{a_1}\Big|_{a_2=0}, \quad S_{21} = \frac{b_2}{a_1}\Big|_{a_2=0}, \quad S_{12} = \frac{b_1}{a_2}\Big|_{a_1=0}, \quad S_{22} = \frac{b_2}{a_2}\Big|_{a_1=0} \qquad (2.11)$$

S_{11}: input reflection coefficient with output matched.
S_{21}: forward transmission coefficient with output matched. Represents the gain (amplifier) or attenuation (passive network).
S_{12}: reverse transmissioncoefficient with input matched.
S_{22}: output reflection coefficient with input matched.

The two port network can now be replaced by a flow graph of S-parameters.

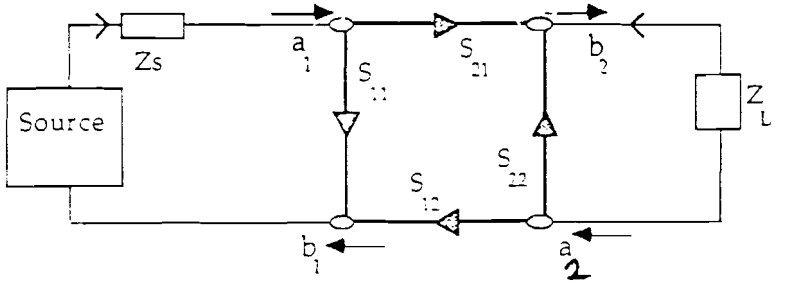

Figure 2.4: S-parameter flow graph

In the measurement of small devices (e.g. MMICs), it is often necessary to embed them into transmission line structures to make connection of the connectors possible. Embedding the device in a transmission line structure changes the reference plane.

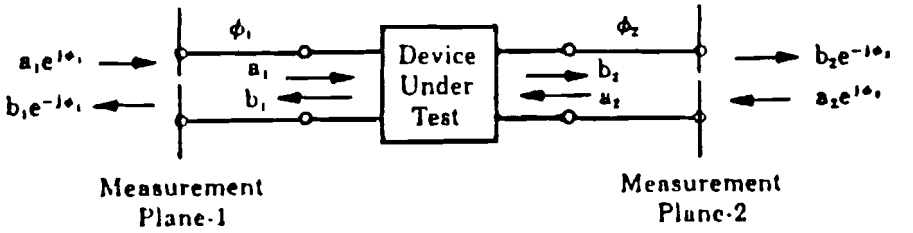

Figure 2.5: DUT embedded in transmission line

See for example Figure 2.5. At port 1 a linelength Φ_1 is added, and at port 2 a linelength Φ_2 is added.

The measured S parameter matrix **S'** is related to the S-parameter matrix **S** of our device by:

$$\mathbf{S'} = \mathbf{\Phi} \cdot \mathbf{S} \cdot \mathbf{\Phi} \tag{2.12}$$

$$\mathbf{\Phi} = \begin{pmatrix} e^{-j\Phi_1} & 0 \\ 0 & e^{-j\Phi_2} \end{pmatrix} \tag{2.13}$$

From the measured S' parameters the S-parameters of our device can be determined with the relationship:

$$\mathbf{S} = \mathbf{\Phi}^{-1} \cdot \mathbf{S'} \cdot \mathbf{\Phi}^{-1} \tag{2.14}$$

In most real situations it is much more difficult to know the effects, influences and performances of the interface between the device under test (DUT) and the reference plane of actual measurement.

2.4 MICROWAVE SWITCH ANALYSIS

Analysis and characterization of the realized devices is needed to optimize the switch performance. One of the most important performance characteristics of the switch is the ON/OFF-Ratio. A good switch should transmit little or no signal-energy in the "off"-state and much signal-energy in the "on"-state. The ON/OFF-Ratio defined in equation 2.15 as the ratio between the transmission coefficient in the "on"-state and the transmission coefficient in the "off"-state, should be as large as possible.

$$On/Off\text{-}Ratio = \frac{S_{21\,ON}}{S_{21\,OFF}} \quad \equiv\equiv\equiv> \quad 20\ Log\left|\frac{S_{21\,ON}}{S_{21\,OFF}}\right|\ dB \tag{2.15}$$

To optimize the ON/OFF-Ratio the optoelectronic microwave switch can be characterized by an equivalent circuit, as is done for example in Figure 1.5, Chapter 1. These simplified equivalent circuits (Figure 1.5) can very well be used to explain the principle of the optoelectronic microwave switch. However, they are not accurate enough to use for simulation and optimization purposes. Several authors published papers about equivalent circuits for the gap discontinuity ([21],[22],[23]). They all analyzed the gap discontinuity using quasi-static methods. The results are used extensively in computer aided design and simulation software.

If the dimensions of the discontinuity are much smaller than the wavelength in the microstrip, the discontinuity may be approximated by an equivalent circuit of lumped elements. For example at 10 GHz the wavelength of the signal is in the order of millimeters, while a discontinuity normally is in the order of micrometers.

Near a discontinuity the electric and magnetic field distribution are modified. The altered electric field distribution gives rise to a change in capacitance, and the changed magnetic field distribution can be written in terms of an equivalent inductance. The gap discontinuity especially introduces a change in electric field distribution.

The gap discontinuity is normally represented by an equivalent π-network of capacitances as shown in Figure 2.6.

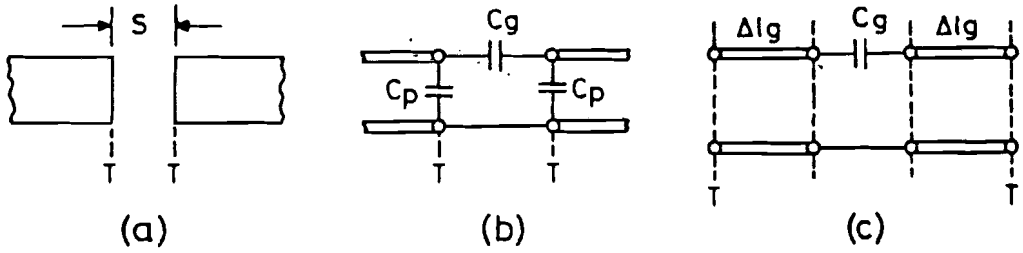

Figure 2.6: Equivalent gap circuits.

The series gap capacitance C_g arises from the coupling effect of the adjacent strip conductors. The shunt capacitances C_p can be inferred from the effect of disorder of the electrostatic field distribution at the edge of the strip conductor. Eventually the shunt capacitances can be replaced by equivalent line lengths l_g.

$$\Delta l_g = C_p \frac{c\, Z_0}{\sqrt{\epsilon_{re}}} \tag{2.16}$$

c: speed of light in vacuum.

In literature closed form expressions are given for C_p and C_g. These expressions will be used to calculate the initial values of the capacitances used in the simulations (see Appendix D).
If the gap is illuminated, free electron-hole pairs are created resulting in a surface conductivity over the gap (photoconductive effect). Thus in the "on"-state the equivalent gap circuit changes as is shown in Figure 2.7:

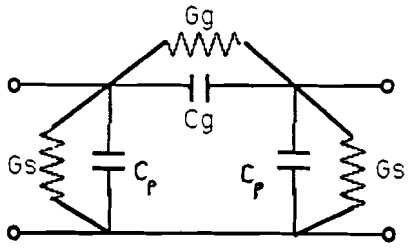

Figure 2.7: Equivalent gap circuit On-state.

Illuminating the gap adds the conductances, but does not change the values of the capacitances in the equivalent circuit. The gap conductance, C_g, can be calculated as:

$$G_g = \frac{W\,\Delta\sigma_s}{\alpha\, l_g} \qquad (2.17)$$

W: gap width
l_g: gap length
α: absorption coefficient
$\Delta\sigma_s$: surface conductivity (see equation 1.5)

This gap conductance is the most influential difference between the equivalent circuit in the "on"-and "off"-state. From equation 2.17 it is clear that the gap conductance can be influenced by changing l_g. The gap width, W, can not be changed, because it must make sure that the characteristic line impedance is 50 Ω.

The principle of the optimization of the ON/OFF-Ratio is to analyse the characteristics of the switch in the "off"-state and to simulate these characteristics with the equivalent π-circuit. The values of the capacitances in the equivalent circuit do not change in the "on"-state. This implies that the change in transmitted signal-energy is due to the gap conductance only, which is directly related to the gap length.

This report treats the characterization at high frequencies of microwave switches in the "off"-state. It is very difficult to perform accurate measurements at these high frequencies, particularly with the non-coaxial transmission media in which the switches are mounted. Part of this report will describe the different measurement methodes and de-embedding techniques.
After characterizing the optoelectronic microwave switches in the "off"-state, the "on"-state must be characterized. The full characterization of the switch in the "on"-and "off"-state is subject of the Thesis of S.Sani (Eng.).

CHAPTER 3

MICROWAVE DEVICE MEASUREMENTS

3.1 INTRODUCTION

In Chapter 2 we saw that microwave devices are normally characterized using S-parameters. The S-parameters can be measured in the frequency-domain by vectorial and scalar high frequency measurement systems. High-frequeny microwave device measurements can also be performed in the time-domain.

Time-domain measurements can provide results that are hard to obtain with frequency-domain measurements. In the time-domain it is very easy to dissociate different discontinuities, to derive their exact location in the DUT (Device Under Test). It is also very easy to measure weak discontinuities. In turn, in the frequency-domain the precision of the measurements, and the signal-to-noise ratio is much better.

Because time-domain and frequency-domain analysis are two additional measurement methods we also performed time-domain measurements. The Time Domain Reflectometry (TDR) method used, provides information about the gap-devices (in the fixture) that is hard to get with frequency-domain measurements.

In the next two paragraphs the principles of time-domain reflectometry and frequency-domain analysis will be explained.

3.2 TIME DOMAIN REFLECTOMETRY

Time-domain measurements appeared in the sixties, when power sources became available that could produce step functions with very short rise times, and oscilloscopes with which signals of over 10 GHz could be observed [26].

The principle of Time Domain Reflectometry (TDR) is to send a known signal in the unknown DUT and to analyze the different reflections due to the discontinuities. The amplitude of the reflected signal corresponds directly to the impedance of the discontinuity. The distance to the reflecting impedance can be determined from the time the pulse needs to return. This is the same principle as for example radar, but here it is in a guided environment.

The TDR method is limited by the minimum system rise time: t_r. A fast rise time allows identification of discontinuities that are close together.

The distance to a discontinuity is given by:

$$d = v_p \cdot t_0/2 \tag{3.1}$$

$v_p = c/\sqrt{(\epsilon_{re})}$: phase velocity in medium.
$t_0 = 2L/v_p$: elapsed time between generated and reflected pulse (L: distance to discontinuity).

The minimum distinguishable distance between two discontinuities is:

$$d_{min} = v_p \cdot t_r/4 \tag{3.2}$$

In the ideal case, $t_r = 0$, we have three basic possibilities:

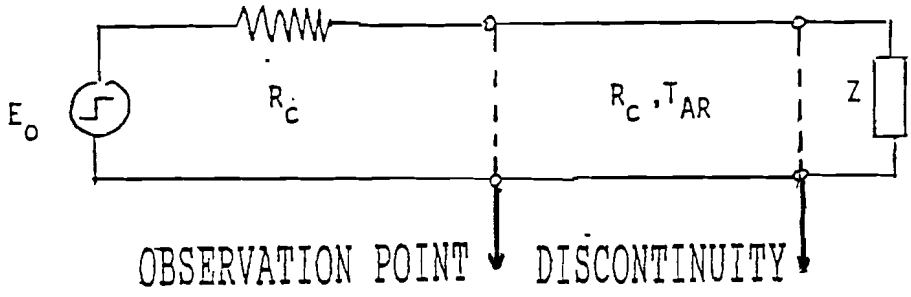

Figure 3.1: TDR measurement diagram

1) Z = R; a purely resistive load. As can be seen from Figure 3.1 a step signal is applied, and the characteristic impedance of the generator and line are the same (e.g. R_c = 50 Ω). The magnitude of the step caused by R is:

$$\rho = \frac{R-R_c}{R+R_c} \tag{3.3}$$

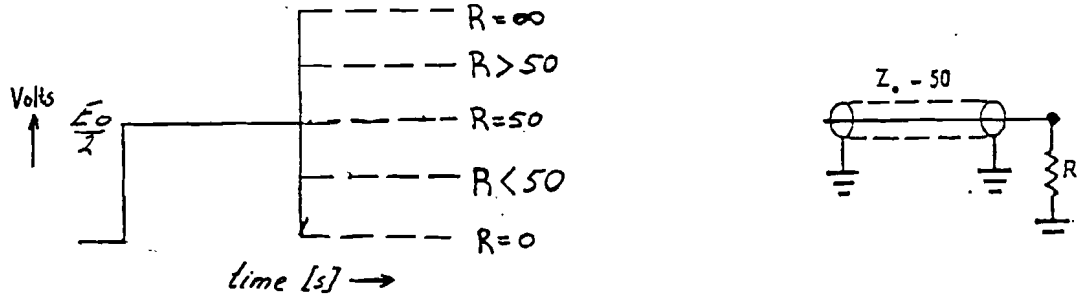

Figure 3.2: Resistant TDR-respons.

2) $Z = R + j\omega L$; The signal front will see Z as an open circuit ($dV/dt = \infty \Rightarrow \omega = \infty \Rightarrow Z = \infty$), and then the inductance will be charged over the resitance ($R + R_c$).

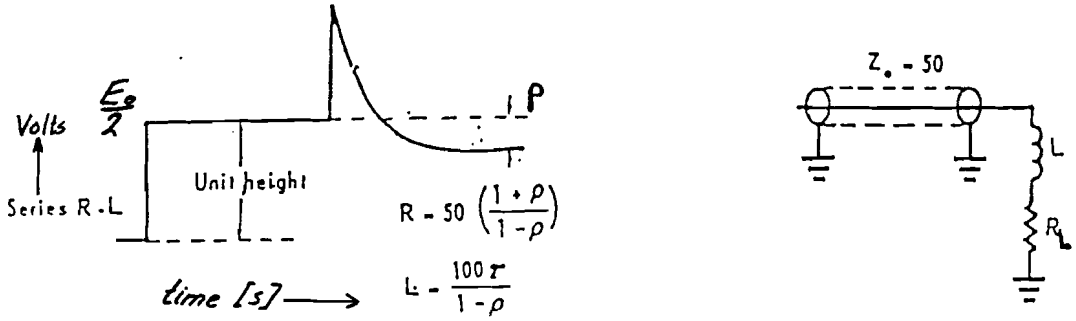

Figure 3.3: TDR-respons of ($R + j\omega L$)

$$V(t') = \frac{E_0}{R+R_c}(R + R_c e^{(-t'/\tau_L)}), \quad \textit{time constant: } \tau_L = \frac{L}{R+R_c} \tag{3.4}$$

3) $1/Z = 1/R + j\omega C$; The signal front will see Z as a short circuit, and then the condensator will be charged over the parallel resistant $R//R_c$.

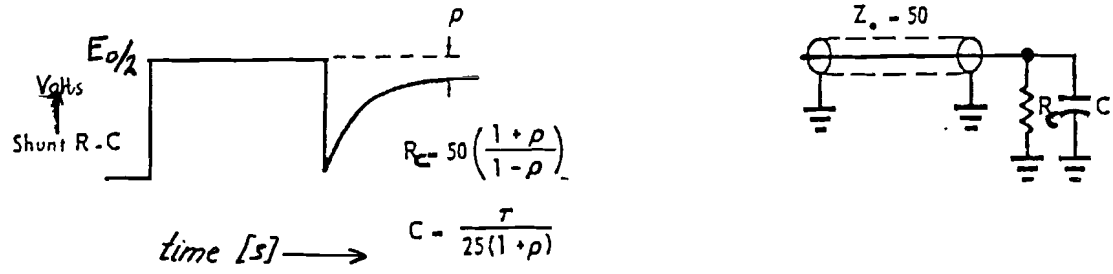

Figure 3.4: TDR-respons (R//C)

$$V(t') = E_0 \frac{R}{R+R_c}(1 - e^{(-t'/\tau_C)}), \quad \textit{time constant: } \tau_C = \frac{C\,R\,R_C}{R+R_C} \tag{3.5}$$

However in real TDR systems the rise time of the input wave is not zero. We can distinguish three cases:

Strong Discontinuity: $t_r << t_0$, and $t_r <<$ time constants ($\tau_{L,C}$).
A strong discontinuity can be analyzed by measuring the amplitude and t_0 directly.

Impossible Discontinuity: $t_r >> t_0$.
The reflected signal is too close to the incident signal and can therefore not be dissociated. The same problem appears when two discontinuities are too close together (distance x too small). Then $x \cdot t_0 < t_r$, and only a global effect of the discontinuities can be measured.

Weak Discontinuity: $t_r < t_0$, and $t_r >$ time constants. This is the most common case. The response of a weak capacitive discontinuity compared to a strong capacitive discontinuity is shown in Figure 3.5.

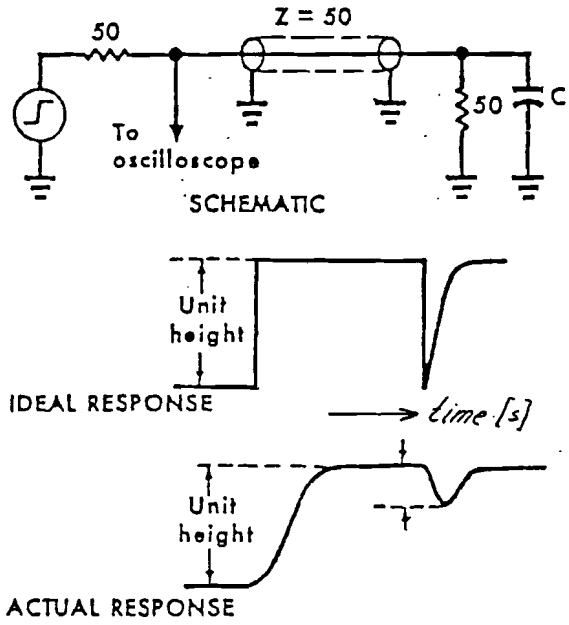

Figure 3.5: Ideal and real TDR-response of a shunt capacity

The discontinuity can be analyzed by presuming the following steps:[25],[27]

$$\rho = \frac{E_r}{E_i} = \frac{(j\omega L + R_c) - R_c}{(j\omega L + R_c) + R_c} \approx \frac{j\omega L}{2R_c} \qquad (3.6)$$

$$\equiv\equiv\equiv> \quad \textit{time domain:} \quad E_r(t) = \frac{L}{2R_c}\frac{\partial}{\partial t}E_i(t)$$

$$\textit{with:}\ S = \frac{\partial E_i}{\partial t} \equiv\equiv\equiv> \quad L = \frac{2R_c E_r}{S} \qquad (3.7)$$

$$\textit{Analog:} \qquad C = -\frac{2E_r}{sR_c} \qquad (3.8)$$

The assumptions ($R_c >$ ωL and $t_r >$ time constant) have to be checked after the calculation of the discontinuity impedance.

The TDR measurements are performed at LHOG (Laboratoire d'Hyperfréquence et d'Optique Guidée) with a Tektronix 7854 Time Domain Analyzer. The system rise time is t_r= 40 ps, and E_0= 500 mV. TDR measurements are performed to get an indication of the discontinuities introduced by the fixtures of the components. The

3.3 FREQUENCY DOMAIN ANALYSIS

Frequency respons of the DUT can be obtained by performing a Fourier Transformation of the time domain response. However S-parameters can be measured directly in the frequency domain by scalar and vectorial analyzers. These high frequency measurement systems are able to deliver a constant power over a large frequency range and contain directional devices to seperate incident and reflected signals.

The HP 8510 B Vectorial Network Analyzer, used at LEMO and LHOG, is one of the best known high frequency measurement systems. The system is built up of a microwave power source, a test set, a display and processor, and a detector. Printers, plotters etc. can be connected also.

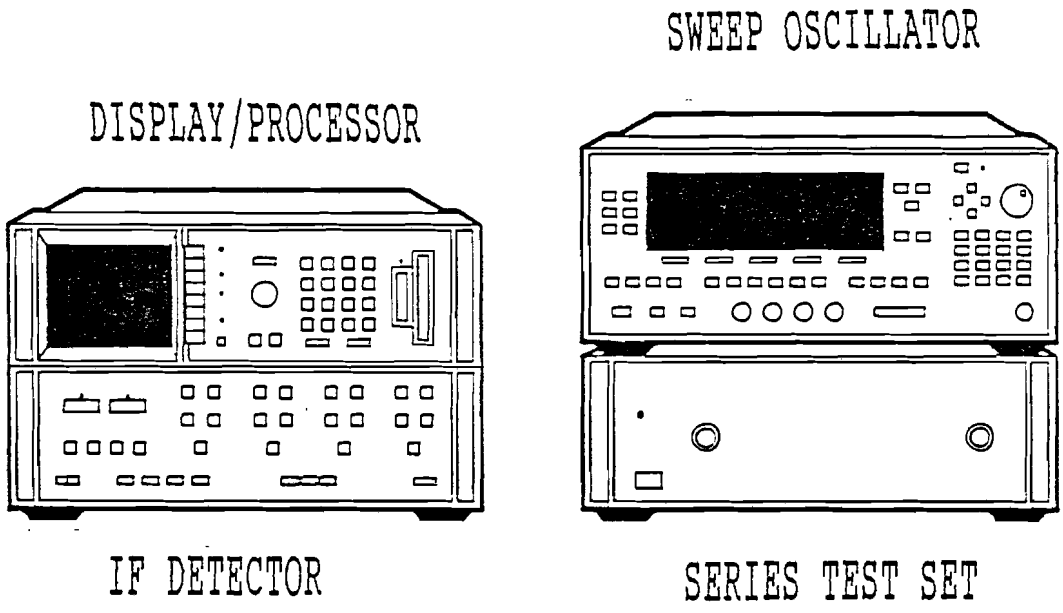

Figure 3.6: The HP 8510 B Network Analyzer

The S-parameters are always measured with respect to a certain reference plane. Without knowing where the reference plane is, the measurements do not have any meaning. The performance of the Network Analyzer (NA), and especially its precision, is primarily limited by the systematic errors introduced by the system. If the system characteristics up to the desired reference plane are wellknown, the introduced systematic errors can be modelled. This is done by a calibration procedure. A calibration makes automatic error correction up to the desired reference plane possible, and therefore improves the precision and validity of the measurements enormeously.

The installation of a calibration (or a systematic error correction function) can be effectuated by a series of particular measurements of wellknown standard devices. The precision with which these standards are known determines the quality of the calibration, and thus of the measurements of the DUT.

The standards to make a normal coaxial calibration are commercially available in calibration kits. A calibration kit contains open circuits, short circuits, matched loads, attenuators etc.. A calibration is valid as long as the reference plane is not changed and the physical environment of the DUT is not modified. For example the phase of the signals is very sensitive to deformation of the 50 Ω coaxial cables that connect the DUT to the test ports. Great care must be taken not to change the position of the cables between the calibration installation and the actual measurements. Even with the greatest care a calibration does not stay accurate for more than a few days.

To make network measurements in microstrip, coplanar waveguide (CPW) or any other non-coaxial media possible, the non-coaxial DUT has to be mounted into a fixture. The fixture makes the non-coaxial-to-coax transition possible. To measure the non-coaxial DUT parameters we need to separate the effects of the transition medium (fixture and system) from the DUT characteristics. This is called de-embedding. There are different de-embedding techniques, which depend on the place of the reference plan. Because the systematic errors are corrected for to the level of the reference plane. See Figure 3.7.

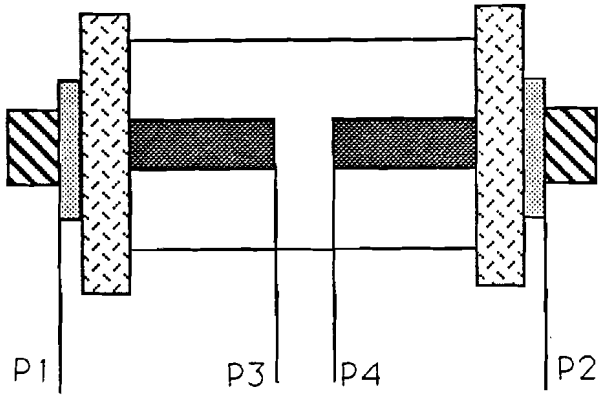

Figure 3.7: The gap-device in the fixture

The difference between the reference planes P1-P2 and P3-P4 makes that the systematic errors at both planes are different also. Before describing methods to model them, which can be done with different calibration methods, the systematic errors and their physical origin will be evaluated.

3.3.1 Systematic errors

Systematic errors are repeatable errors due to the measurement system and its interaction with the test device. Connectors, adapters and other transition components can also introduce repeatable errors. Basically the systematic errors are due to: lack of directivity, load and source impedance mismatches, bad isolation and tracking errors.[28],[29]

In general a DUT is characterized by its reflection and transmission coefficients. The systematic errors can therefore also be divided in reflection measurement errors and transmission measurement errors.[30]

Reflection Measurement Errors

To measure reflected signals a directional device is needed to separate the reflected signal from the incident signal. The precision of the reflection measurement is limited by the directional coupler and the system in which it is used. The basic principle of reflection measurements is shown in Figure 3.8.[29]

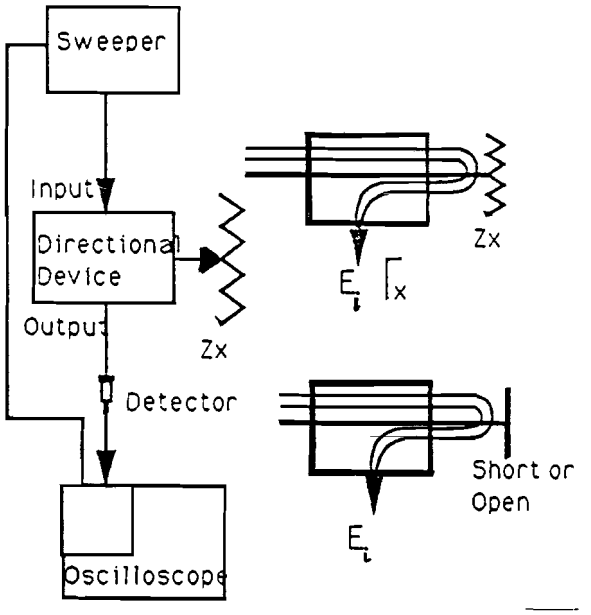

Figure 3.8: Priciple of reflection measurements

It consists of connecting the unknown device at the directional coupler which receives a signal from a source. The output of the directional coupler is visualized on an oscilloscope. The comparison of this reflected signal with the signal of a total reflection gives the reflection coefficient: Γ (dB). Two characteristics of the directional coupler influence the precision of the measurement:

1) The Directivity
2) Mismatch of the source and test set.

The Directivity Error

If an adapted load Z_0, with an impedance equal to the impedance of the acces port is connected, the load will absorb all the incident energy. There will be no energy reflected to the directional coupler. However, at the output there is some energy measured which obviously did not reach the load (See Figure 3.9). This part is defined as the directivity: E_d.

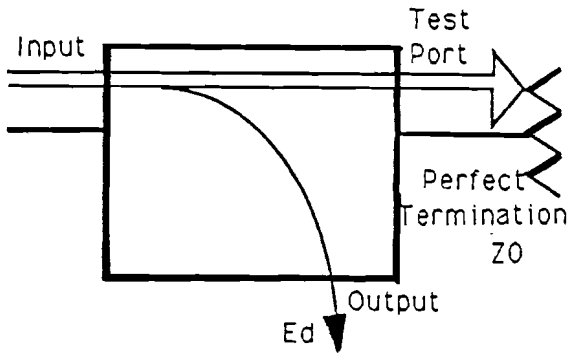

Figure 3.9: The Directivity Error

The directivity of a device results from:
-differences of the intern geometry of the reflectometer compared to the ideal case.
-mismatches of connectors.
-imperfect intern terminations.

It is difficult to extract the reflection coefficient of an unknown load, because the reflection coefficient is always measured in combination with the directivity.

By using a total reflect (0 dB) the directivity can be measured easily as the amount of dB's below 0 dB. In Figure 3.10 is shown in what way the directivity influences a reflection measurement.

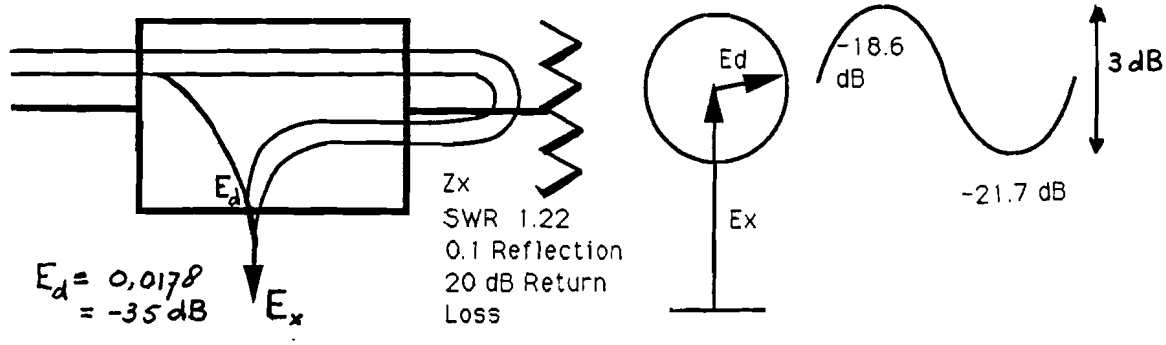

Figure 3.10: Influence of directivity error on reflection measurements

In this example the unknown load has a SWR of 1,22 which equals a 20 dB Return Loss. The directivity is chosen to be 35 dB under the level of total reflection, or 0,0178 of a totally reflected signal. Figure 3.10 shows in what way the phase vectors can be combined. Instead of measuring a reflection coefficient of 20 dB the measured value will be something between:

$$-21{,}7 \text{ dB} < E_m < -18{,}6 \text{ dB } (= 20 \text{ Log } \{0.1 + 0.0178\}).$$

This means an absolute uncertainty of measurement of more than 3 dB.

The second error due to the characteristics of the directional coupler is the mismatch of the test set interface.

Test Set Interface Mismatch

If a total reflect (open or short circuit) is connected the totally reflected signal sets the reference output level at 0 dB. However if the test set interface reflects part of the reflected signal (Γ_{st}) as a result of the mismatch, this part will be totally re-reflected towards the test set with a reflection Γ_{st} under the 0 dB reference level. This Γ_{st} dB level is then superimposed on the 0 dB reference (see Figure 3.11).

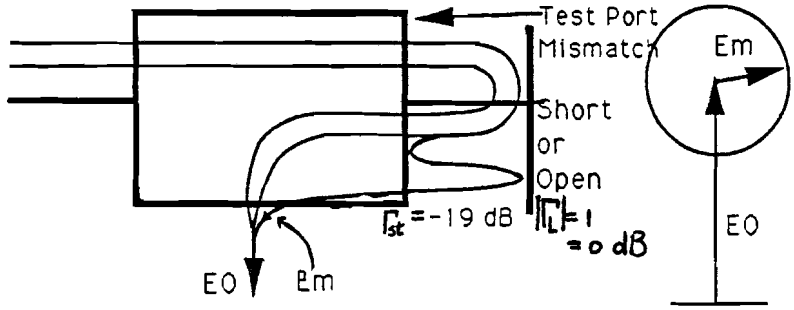

Figure 3.11: Test port interface mismatch

The better the adaptation of the load (Γ_L small), the smaller the error made. The error is: $\Gamma_{st}\Gamma_L^2$. Thus, it is preferable to evaluate this error with a load with a large reflection coefficient (Total Reflect: $\Gamma = 1$ (0 dB)).

The third error that influences the reflection measurements is the system source mismatch.

Source Mismatch

The source mismatch is due to the fact that the source is never adapted perfectly. If a total reflection is connected the incident signal will be totally reflected (0 dB). However part of the reflected signal (Γ_s) will be re-reflected towards the open or short circuit as a result of the source mismatch (see Figure 3.12).

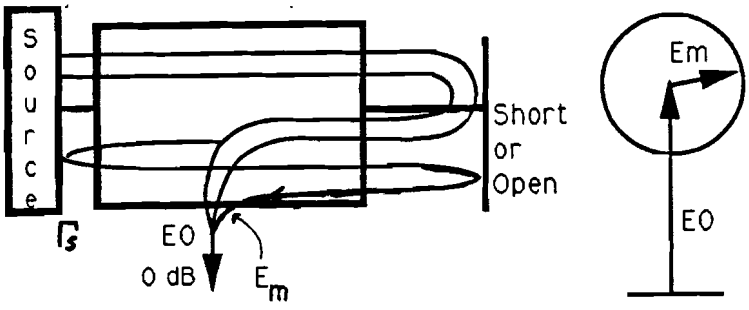

Figure 3.12: Source Mismatch

Transmission Measurements Errors

The transmission errors are mainly introduced by detector-source mismatches, see Figure 3.13.

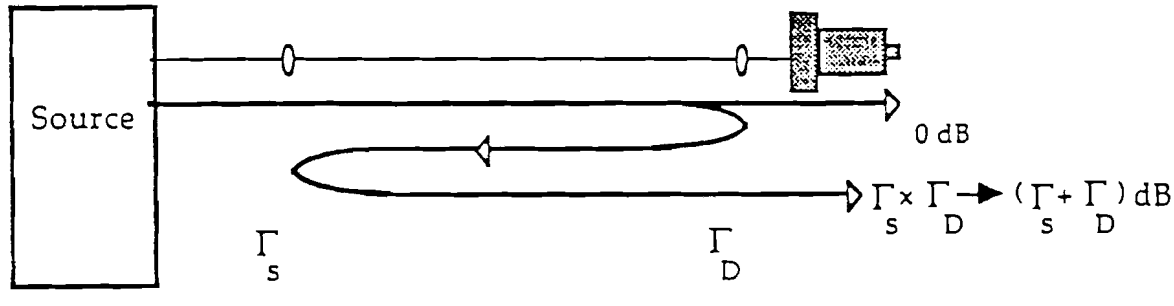

Figure 3.13: Detector-Source Mismatch

If the source is connected directly to the detector we see that the source and detector mismatches, translated to reflected losses in dB, can be added. If the DUT is added, its attenuation will contribute twice to the diminuation of the interaction between source and detector. The biggest transmission error occurs if a DUT is measured with a very high or very low insertion loss.

A second transmission measurement error is the isolation.

Isolation
The isolation error is caused by interference between incident signals and transmitted signals, mainly inside the measurement equipment. But also as a result of coupling between the two measurement points which can be very close together (e.g. in on-wafer measurements).

3.3.2 Error models

Now the physical origin of the systematic errors is known, correction methods can be designed to make it possible to extract the intrinsic DUT S-parameters from the overall measured characteristics. These correction methods all rely on error models representing the systematic errors together with the S-parameters in flow graphs.

Several error models may be used to correct the measurements, depending on the desired precision, calculation time, available memory etc.. The most used error models are the 8-term and the 12-term model in two port networks [12],[19].

The 8-term error model consists of two error boxes, Q_A and Q_B, at each access to the DUT. These two boxes contain all the systematic errors.

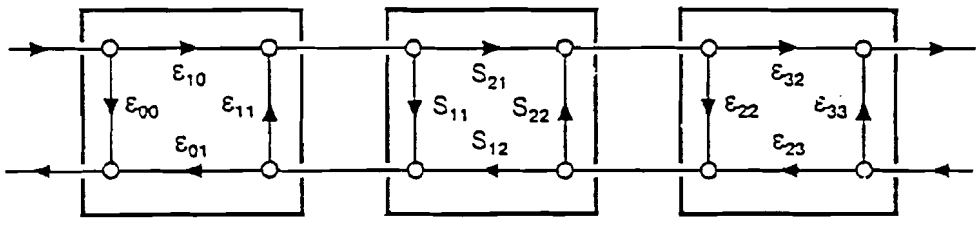

$\varepsilon_{10}\,\varepsilon_{01} = E_{RF}$
$\varepsilon_{00} = E_{DF}$
$\varepsilon_{11} = E_{SF},\ E_{LR}$
$\varepsilon_{10}\,\varepsilon_{32} = E_{TF}$

$\varepsilon_{23}\,\varepsilon_{33} = E_{RR}$
$\varepsilon_{33} = E_{DR}$
$\varepsilon_{22} = E_{SR},\ E_{LF}$
$\varepsilon_{01}\,\varepsilon_{23} = E_{TR}$

Figure 3.14: 8-Term Error Model

The 12-term error model is also called a 12-term universal model. It is the most complete existent error model and is based on the physical model of the measurement system. It takes into account all the systematic errors as described in paragraph 3.3.1. To calculate only one intrinsic S-parameter S_{ij} all four S-parameters S_{ijm} should be measured. This 12-term error model is the model used by the HP 8510 B NA.

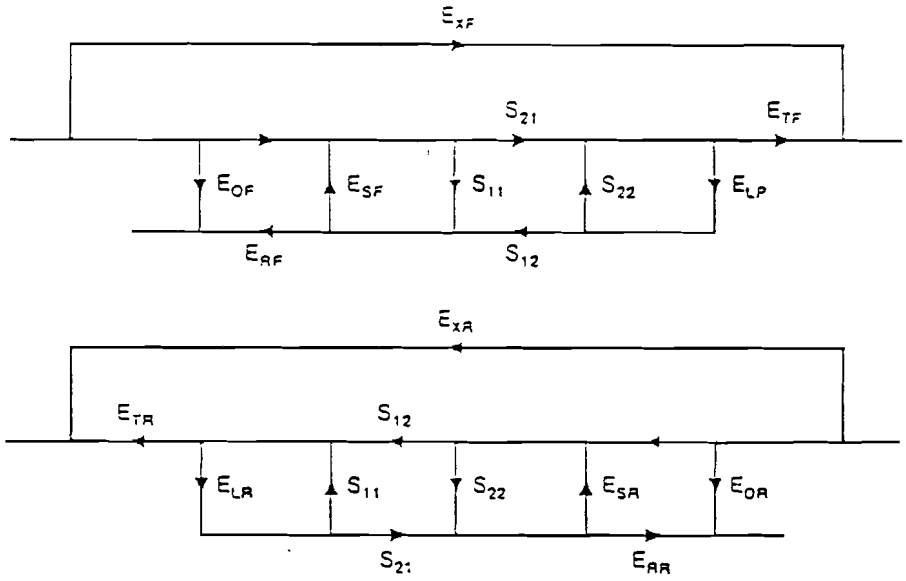

E_{DF}, E_{DR} – Directivity
E_{SF}, E_{SR} – Source Match
E_{XF}, E_{XR} – Isolation
E_{TF}, E_{TR} – Trans. Tracking
E_{RF}, E_{RR} – Refl. Tracking
E_{LF}, E_{LR} – Load Match

Figure 3.15: 12-Term Error Model

The advantage of the 8-term error model is that it requires less error terms. Furthermore with one simple reflection measurement on one port the directivity of the system and the source mismatch are known. This decreases calculation time and mass storage. Nowadays, with the relatively cheap memory and processors, this is not of great

importance anymore. However the 8-term error model is still a popular tool of describing S-parameter measurements with errors.

The determination of the values of the terms in the error model is done by the calibration. There are several calibration methods possible, dependent on where the reference plane is located.

3.3.3 Calibration and de-embedding

During the calibration phase the Reference Plane is situated. The S-parameters are measured relative to the reference plane. Often the scattering parameters of the DUT have to be de-embedded from the overall measured parameters. Thus the de-embedding method depends on the place of the reference plane. There are mainly two de-embedding methods:

1) Two-Tier De-embedding.
2) One-Tier De-embedding.

Two-Tier De-embedding
In non-coaxial measurements it is difficult to build precision impedance standards for calibrating a network analyzer (NA). They are not commercially available neither. In this case two-tier de-embedding can be used.

The two-tier de-embedding method, illustrated in Figure 3.16, consists of [13],[15]:

1) Calibrating the NA using normal coaxial standards.
2) Using the calibrated NA to characterize the fixture by a lumped equivalent circuit model.
3) By placing the DUT in the fixture instead of the fixture standards, the DUT S-parameters can be de-embedded from the overall measured S-parameters using matrix analysis.

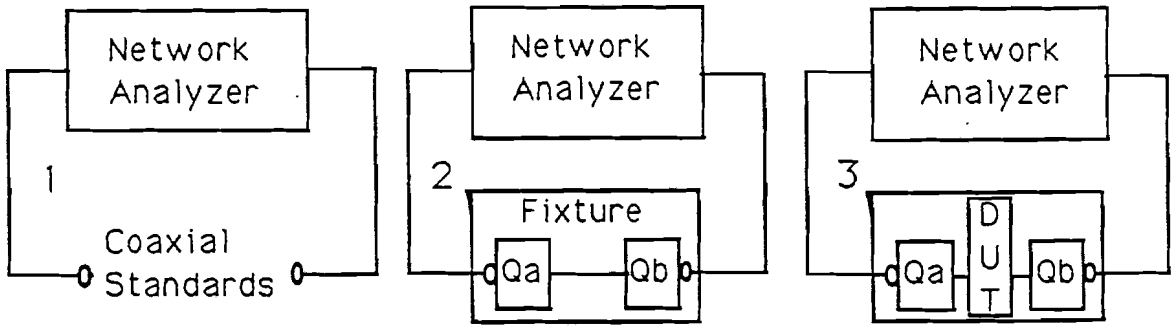

Figure 3.16: Two-Tier De-embedding

This de-embedding method is used succesfully to characterize active devices as GaAs MESFETs [11],[15]. Simons and Ponchak [13] have modeled succesfully CPW discontinuities using two-tier de-embedding. The equivalent circuit model of the CPW fixture used by them is shown in Figure 3.17.

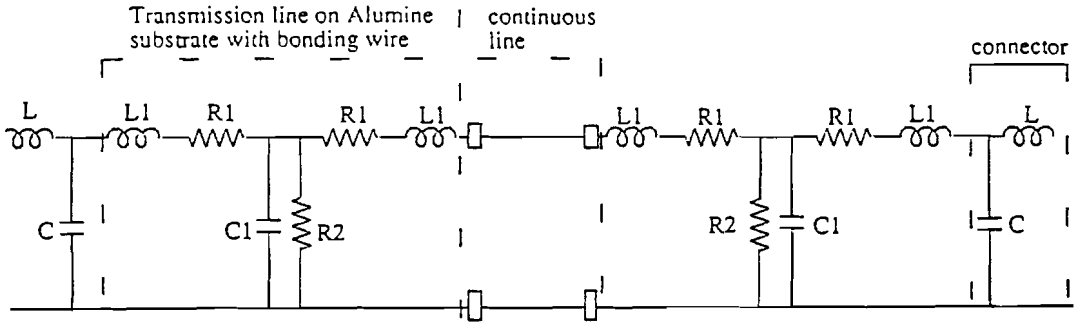

Figure 3.17: Equivalent circuit of continuous line in fixture [13]

The values of the elements in the equivalent circuit can be found by using optimization software (SuperCompact, MDS). This model may be used to de-embed the characteristics of our gap device on Cr:GaAs-substrate from the overall characteristics.

The two-tier de-embedding method can be used if a low-loss, well-matched fixture can be constructed. However, especially at higher frequencies the test fixture can no longer be considered ideal, and will exhibit impedance discontinuities and attenuations too complex to model conveniently. If a valable equivalent circuit of the test fixture cannot be found this method cannot be used.
Another problem may be that the model does not take into account the geometrical errors of the test fixture.

One-Tier De-embedding

Calibrating the NA and fixture using standards in the medium of the DUT (microstrip, CPW) is called one-tier de-embedding. The relavant steps are shown in Figure 3.18.

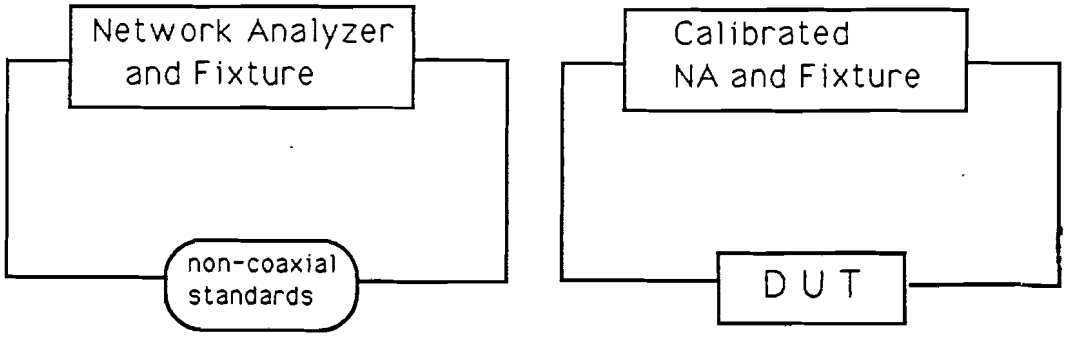

Figure 3.18: One-Tier De-embedding

Instead of precisely known impedance standards, transmission lines are used for the calibration. This offers the following advantages:

1) Transmission lines are relatively simple to realize.
2) The transmission line characteristic impedance can be accurately determined from physical dimensions and the used substrate materials.
3) Transmission lines are often used as standards and are well understood.
4) The reference plane can now be placed after the coax-to-non-coaxial transition (level P3-P4, Figure 3.7), so its systematic errors are automatically taken into account.

The first methods used only two non-coaxial line standards. They can be called Through-Delay Calibration. These methods use 8-term error models. They assume the two ports identical (reciprocal) and perfectly isolated. They use simplified mathematical expressions [18]. At low frequency ranges this gave good results.

In 1975 a new method, called TSD (Through, Short, Delay) was presented [14]. It uses a perfect short circuit. A perfect short circuit is difficult to realize, which is a disadvantage of the TSD calibration method.

In 1979 the TRL (Through, Reflect, Line) Calibration method was introduced by Engen and Hoer [17]. In addition to the Through and the Line standard this method uses an open circuit: the Reflect. The Reflect must have a very high reflection coefficient which need not to be known precisely. The TRL method uses the 12-term error model. It is the most popular calibration method in one-tier de-embedding cases.

We will use this method in our experiments to measure the S-parameters of a gap-device. We want to measure the S-parameters of a gap in a microstrip line and in a coplanar waveguide (CPW) line on Cr:GaAs substrates, over a frequency range of 0.5GHz - 10GHz. Because these are high frequencies and because the test fixture is large (see Figure 3.17) the two-tier de-embedding technique may not give adequate results.

CHAPTER 4

EXPERIMENTAL AND SIMULATED RESULTS

4.1 INTRODUCTION

The experiments done can be divided in two subgroups:

Epsilam-10 experiments (devices on Epsilam-10 substrate).
Cr:GaAs experiments (devices on Cr:GaAs substrate).

First measurements with Epsilam-10 devices were done. As described earlier, Epsilam-10 has more or less the same physical properties as Cr:GaAs, if the materials are not under illumination (as is the case in the "off"-state). Furthermore the Epsilam-10 devices can be mounted into simple fixtures, while the Cr:GaAs devices need complex fixtures, because of their small dimensions. As a result of these complex fixtures the realization of the TRL standards and the TRL implementation is more complicated too.
The Epsilam-10 experiment serves as a test-case, to see if, and in what way, the TRL-procedure can give satisfying results. In second instance a TRL-procedure for the Cr:GaAs gap-devices could be designed and implemented.

The TRL measurement-results obtained with the Epsilam-10 devices, are compared with measurement-results obtained when a normal coaxial calibration is used. The measurements are also compared with simulations. The simulations are done with the software packets SuperCompact and MDS. This is described in paragraph 4.2.
Paragraph 4.3 describes the realization of the Cr:GaAs devices, and the measurements done with them.

4.2 THE EPSILAM-10 EXPERIMENT

The aim of the experiments with the Epsilam-10 devices, is to investigate the possibilities and performance of high frequency measurements using a TRL (Through-Reflect-Line) calibration. The experiments will also give an indication of the practical problems that have to be faced with the implementation of a TRL-Calibration.
The most obvious problem when implementing a TRL-Calibration, is the need to produce a set of unique standards. For every specific non-coaxial device you want to measure, you need a specific set of standards to implement a TRL-Calibration. This

TRL-Calibration can only be used for that specific non-coaxial device. In case of coaxial measurements, commercially available calibration kits exist containing all kind of standards. With these coaxial standards calibrations can be implemented to perform measurements of all kind of coaxial devices.

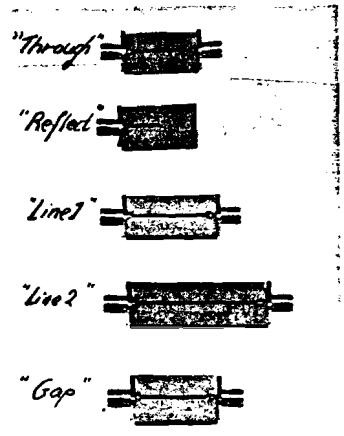

Figure 4.1: Epsilam-10 gap-and standard devices.

The TRL-Calibration uses at least three different (non-coaxial) standards. To make a connection with the coaxial test cables possible, the standards have to be mounted into a fixture. In literature one shiftable test fixture is used for all standards. In this way every standard has exactly the same fixture. At LEMO we do not have such a fixture. We use different fixtures for each standard. In paragraph 4.2.1 and 4.2.2 the Epsilam-10 devices are described. Figure 4.1 shows a photograph of the gap- and standard devices on Epsilam-10.

4.2.1. The Epsilam-10 Microstrip Gap-Device

The Epsilam-10 experiment is set up to see if the intrinsic S-parameters of a microstrip-gap device could be measured conveniently using a TRL-Calibration. The gap-device, and TRL standards, are fabricated on Epsilam-10. Epsilam-10 is an alloy of ceramic and teflon, which combines the physical properties of plastic with the electrical properties of aluminium. To avoid mismatches between the 50Ω-impedance coaxial cables of the Network Analyzer and the microstrip devices, the characteristic impedance of the microstrip devices must be 50 Ω also. By using the SuperCompact Transmission Line Synthesis software a stripwidth of W = 1.18 mm is found (see Appendix B) to assure a 50 Ω characteristic impedance. The transmission lines are assumed to be lossless and non dispersive. Up to 10 GHz this is a valid assumption [9]. The effective relative permittivity, ϵ_{re}, which takes into account the inhomogeneous microstrip structure, is calculated as: ϵ_{re}= 6.8 (Appendix B). The other dimensions are chosen arbitrarily or given by the supplier of the material.
The physical dimensions of the gap component are:

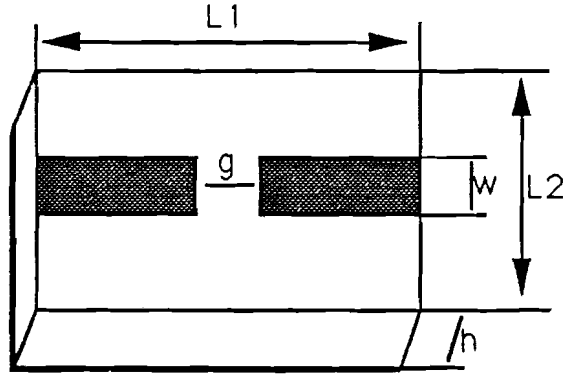

g = 0.2 mm
h = 1.27 mm
ϵ_r = 10
ϵ_{reff} = 6.8
t = 35 μm
W = 1.18 mm
L_1 = 30 mm
L_2 = 20 mm

Figure 4.2: The gap-device

4.2.2 The TRL-Calibration Procedure

The principle of the TRL-calibration method will be described. In [17] a full mathematical solution of the TRL-Calibration is given. As is shown in Figure 4.3 a simplified two-port measurement set up can be represented by two error boxes, Q_A and Q_B, at both sides of the DUT.[12]

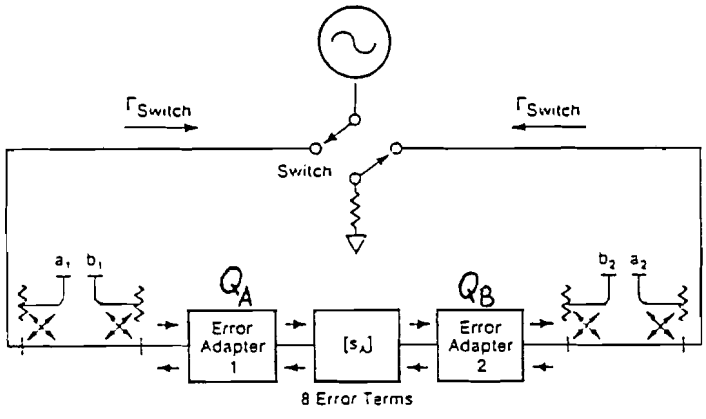

Figure 4.3: Block diagram for a two-port error-corrected measurement system

The eight error terms in these boxes (see also Figure 3.14) can be characterized by the TRL-calibration method.

The VNA uses the 12-term error model. The 12 error terms can be partly derived from the 8-term error model. To solve the eight error terms at least eight independent equations are required. In the basic TRL procedure ten measurements are made, resulting in ten independent equations instead of eight. This is why two more device constants can be derived. In the TRL procedure the complex reflection coefficient of the Reflect Standard and the propagation coefficient of the Line Standard are determined. These characteristics do not have to be specified in advance as in other calibration methods where the accuracy is dependent on how well these characteristics are known.

At this point the eight error term model is solved. Two additional steps are needed to complete the calibration. Forward and reverse isolation is measured as the leakage from port 1 to port 2 with each port terminated. Furthermore, in the 8-term error model ϵ_{11} and ϵ_{22} present both source and load match. However, in any switching test set (see figure 4.3) the terminating switch impedance is different if the switch position is changed from port 1 to port 2. By measuring the ratio of the incident signals a_1 and a_2 during the Line and Through step the switch impedance is measured and used to modify ϵ_{11} and ϵ_{22}. ϵ_{11} is modified to produce the forward source match (E_{sf}) and reverse load match (E_{lr}). ϵ_{22} is modified to produce reverse source match (E_{sr}) and forward load match (E_{lf}).

In the next three sections the physical dimensions of the used standards will be described, as well as the flow graph with the eight term error model.

4.2.2.1 Through Standard

The implementation of a TRL is the simplest if a zero-length Through can be realized. However, sometimes a non-zero-length Through is required. For example, if calibrating coaxial test ports of the same sex, a direct Through connection is impossible.

In our case a zero-length Through Standard is fabricated by connecting P3 and P4 directly (see Figure 4.4). The dimensions will be:

$L_1 = 29{,}8$ mm.
$L_2 = 20$ mm.

The flow graph of this standard is given in Figure 4.4.

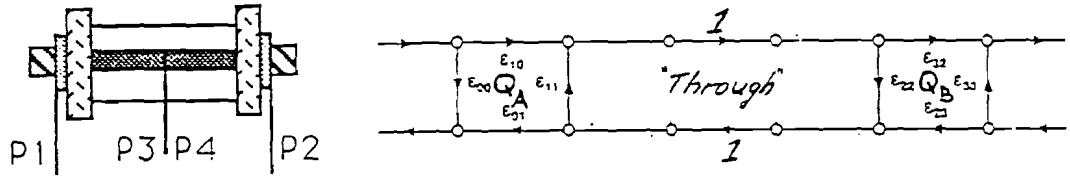

Figure 4.4: Layout and flow graph of the Through standard

With the Through Standard six calibration measurements are made: transmission frequency response and port match are measured in both directions, and the ratio of incident signals (a_1 and a_2) is measured. During the Through Standard measurements the reference plane is set in the middle of the Through line. S_{11} and S_{22} are defined to be zero.

4.2.2.2 Reflect Standard

The zero-length Reflect Standard is an open circuit with a very high reflection coefficient. As is explained before it is not necessary to know the reflection coefficient of the Reflect exactly, as long as it is exactly the same on port 1 and port 2.

The Reflect Standard will be 14,9 mm long and has the following flow graph.

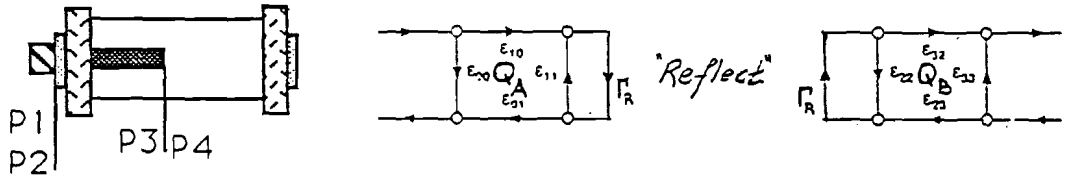

Figure 4.5: Layout and flow graph of the Reflect standard

With the Reflect Standard two reflection measurements are made.

4.2.2.3 Line Standard

The Line Standard seperates the reference points P3 and P4 by a line length L. L introduces a delay and a phase shift. The linelength L must introduce at the beginning and end of the frequency band (0.5 GHz - 10 GHz) a phase shift different from $k\pi$ rad (or k·180°), otherwise the Line becomes transparant with the Through. Because the zero-length Through has an insertion phase of zero degrees.
To be sure it is recommended that the difference in insertion phase is between 20° and 160° (± 180°). So the insertion phase of the Line must be greater than 20° at the start frequency and smaller than 160° at the stop frequency. Because the ratio of the insertion phases at the stop and start frequency is limited by 160/20 = 8, also the frequency range, that can be measured with one Line Standard, is limited by $f_{stop}/f_{start} < 8$. Furthermore the optimal Line length should introduce a 90° phase shift at the center frequency. So the optimal linelength is a quarter wavelength at the center frequency.

$$L_{opt} = \frac{\lambda_g}{4}, \qquad \lambda_g = \frac{v_p}{f_c} = \frac{c}{f_c\sqrt{\epsilon_{re}}}$$

$$\textit{Frequency-band} : 0.5 - 10\ GHz : \quad f_c = 5.25\ GHz \tag{4.1}$$

$$\equiv\equiv\equiv> \quad L_{opt} = \frac{c}{4f_c\sqrt{\epsilon_{re}}} = 5.5\ mm$$

These two conditions define the linelength and the number of lines that have to be used to cover the whole frequency range. The ratio between the stop and start frequency must not exceed 8.

$$\textit{Phase} \quad \theta = \beta L = \frac{2\pi L}{\lambda_g} = \frac{2\pi L}{v_p} f$$

$$\equiv\equiv\equiv> \quad \frac{\theta_2}{\theta_1} = \frac{f_2}{f_1} \le \frac{160}{20} = 8 \tag{4.2}$$

We have to determine whether this 5.5 mm Line meets the condition of acceptable insertion phase.

θ_1 = 8.5 deg at 0.5 GHz
θ_2 = 171.5 deg at 10 GHz

So the 5.5 mm Line Standard does not meet the insertion phase requirements. To cover a frequency span greater than 8:1 more lines must be used. If the span is less than 64:1 then two Line Standards will be sufficient.

The frequency range must be divided allowing one quarter wavelength Line Standard

cover the lower band and a second Line Standard cover the upper band. The optimal break frequency is the geometric mean frequency $\sqrt{(f_{start} * f_{stop})}$:
f_{break} = 2.24 GHz.

Since two Line Standards have to be realized we can conclude to do two seperate TRL-Calibrations. One from 0.5 - 2.25 GHz, and one from 2.25 - 10 GHz with Line2.

The lines are calculated using equation (4.1), as: L_1 = 20.9 mm
L_2 = 4.7 mm

These linelengths meet the condition of insertion phase, and 90° phase shift at the center frequency of their frequency range. The layout and flow graph of the two Line Standards are shown in Figure 4.6.

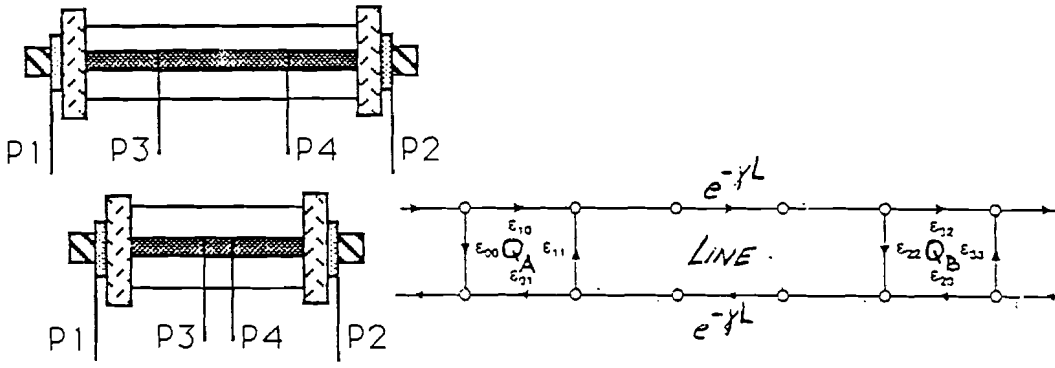

Figure 4.6: Layout and flow graph of the Line standards

The lossless Line Standard introduces a time delay between the reference points. This has to be corrected for by the Network Analyzer. The Offset Delay can be calculated as:

$$\textit{Offset Delay} = \textit{Electrical Length}/\ c = \frac{\textit{Physical Length} * \sqrt{\epsilon_{re}}}{c} \qquad (4.3)$$

Offset Delay Line1 = 182 ps
Offset Delay Line2 = 41 ps

Now the TRL standards are specified, they can be fabricated. The lenght of the acces lines to the reference plane is 14.9 mm. The Through line being the direct connection between P1 and P2 will be 2*14.9 = 29.8 mm long.
The Reflect will be 14.9 mm long.
Line1 will be 2*14.9 + 20.9 = 50.7 mm long.
Line2 will be 2*14.9 + 4.7 = 34.5 mm long.

4.2.3 TDR-Measurements

At first we had problems with the TRL-Calibration implementation. This was probably due to bad coax-to-microstrip transitions and connectors. For this reason the connection of the connectors to the Epsilam-10 substrate and the coax-to-microstrip transition are examined by means of TDR analysis. Also the characteristic impedance of the lines can be obtained, assuming an effective relative permittivity of ϵ_{re}= 6.8 as calculated with closed form expressions (Appendix B). Figure 4.7 shows the time domain respons of the Through Standard.

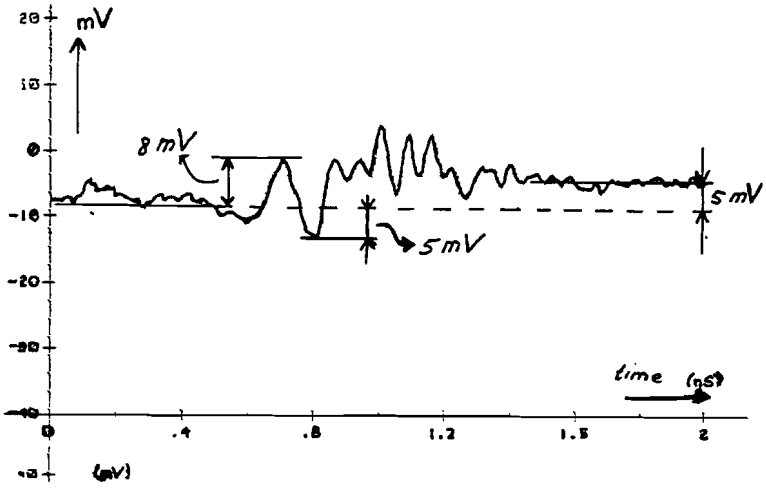

Figure 4.7: Time Domain Respons of the Through Standard Line

The characteristic line impedance can be calculated as:

E_r= 5 mV, E_i=250 mV
= = > Reflection Coeffiecient $|\Gamma|$ = 5/250 = 0.02
= = > SWR=1.02/0.98=1.04
= = > Z_c= 50*SWR = 52.1 Ω

So there is only a slight mismatch with the, in Appendix B, calculated characteristic impedance of 50.5 Ω and the charateristic impedance of the coaxial test cables (50 Ω).

The coax-to-microstrip transition is often modeled by an LC-network as illustrated in Figure 4.8:

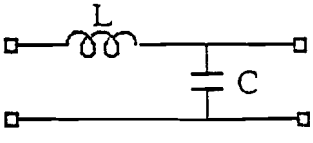

Figure 4.8: Equivalent circuit microstrip-to-coax transition.

$$f_{res} = \frac{1}{2\pi\sqrt{LC}} \qquad (4.4)$$

If the resonance frequency of the transition lies in the measurement frequency range, it decreases the measurement accuracy. The inductance and capacitance can be calculated using equation 3.7 and 3.8, Chapter 3, for weak discontinuities.

$$L = \frac{2R_0E_r}{S}, \qquad C = -\frac{2E_r}{SR_0}, \qquad s = \frac{E_0/2}{T_r} \tag{4.5}$$

==> L = 0.13 nH (E_r= 8 mV) C = 32 pF (E_r= -5 mV)

==> f_{res}= 78 GHz

This results in a f_{res}= 78 GHz. The coax-to-microstrip launch will not seriously influence the measurements. The assumptions made of weak discontinuity were:

1) $R_0 >> \omega L$ $\quad 50 >> 2\pi*10^{10}*0.13*10^{-9} = 8.17$

2) $T_r >$ time constants $\tau_{L,C}$ $\quad 40$ ps $> \tau_{L,C}$
$\tau_L = L/(R+R_l) = 1.3$ ps
$\tau_C = CRR_c/(R+R_c) = 0.8$ ps

So both conditions are met, and the weak discontinuity assumption is justified.

In this experiment every standard has its own fixture and connectors. In literature it is advised to use a commercially available, shiftable fixture in which all standards can be put in. Like this the measurement environment changes as little as possible between the measurements. Figure 4.9 shows the TDR results of the connectors of the Through, Line1 and Line2 Standard. The three transitions show the same behaviour. The differences are within 2 mV, on an incident signal of 250 mV. This is acceptable in the frequency range of 0.5 - 10 GHz, though it might introduce a slight reduction in measurement precision.

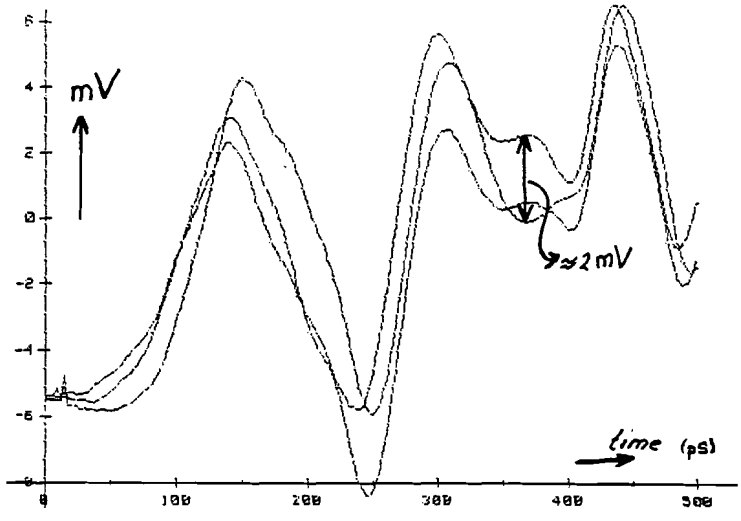

Figure 4.9: Comparison of behaviour of Through, Line1 and Line2 connectors in time domain

4.2.4 TRL Measurements

First a TRL-Calibration of 0.5 - 2.25 GHz is performed with the Line1 Standard (20.9 mm between the reference points P3-P4). Once the TRL standard measurements are made, some confidence in measurement integrity must be derived. In non-coaxial cases normal verification kits do not exist. As a result it will be difficult to state the absolute accuracy.

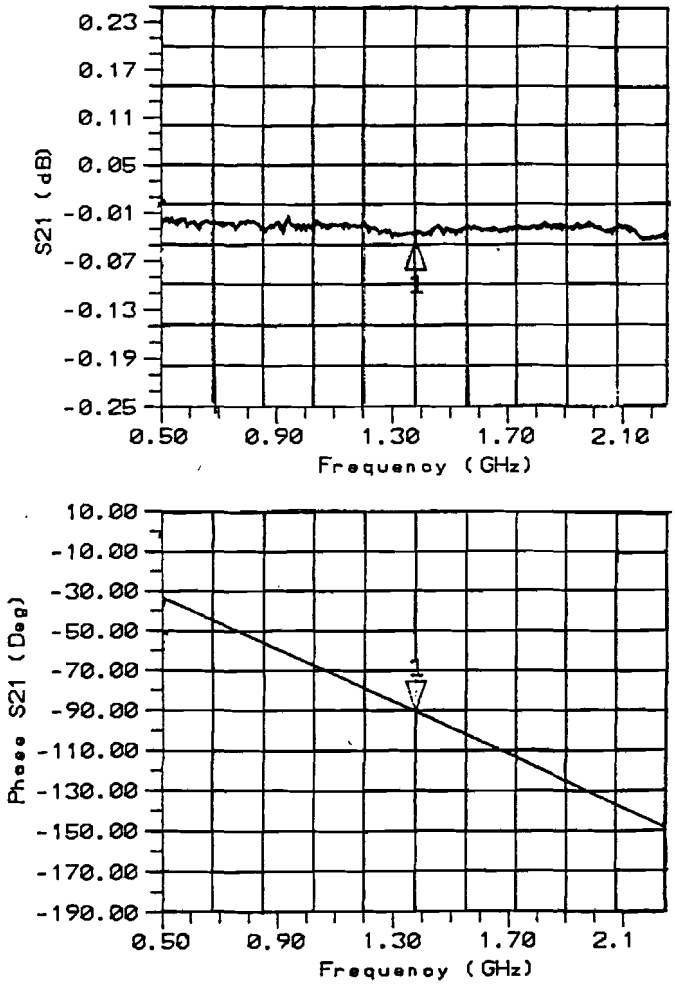

Figure 4.10:a) Magnitude (dB) of the Line1 standard b) Phase (Deg) of the Line1 standard

Measuring well-known devices and comparing the TRL results with the known results can give an indication of the calibration accuracy. Although it is not advisable to test a calibration with the used standards, some measurements can give a good indication of the precision. Figure 4.10 shows the phase and magnitude of the Line1 Standard. As can be seen is the signal power over the whole frequency range better than 0.05 dB, which means more than 99.4 % of incident power (incident on P3) is transmitted (to P4).

A continuous line always transmits almost all incident power, even with bad calibrations. Figure 4.10 only shows that the losses are very little, so nothing is wrong with the transition or connectors. The phase graphic however is interesting, and indicates a good calibration. Figure 4.10b shows that the insertion phase at the frequency band limits is between 20° and 160°, with exactly 90° phase shift at the center frequency. Furthermore the phase shift shows a linear decay with increasing frequency.

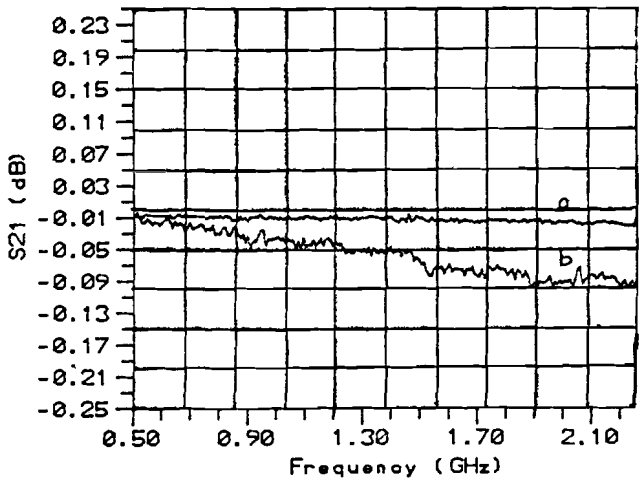

Figure 4.11: Respons of continuous microstrip line ;a) in fixture with TRL b) coax calibration at level of the connectors

In Figure 4.11 the respons of a 0.47 cm (between P3-P4) continuous microstrip line is shown. (In fact this is the LINE2 Standard that is not used in this calibration).
The results of a TRL in-fixture calibration (Reference Plane P3-P4) together with a normal coaxial calibration (Reference Plane P1-P2) are shown. Using the TRL-Calibration the transition loss of the line can be measured directly, without the attenuation due to the fixture.

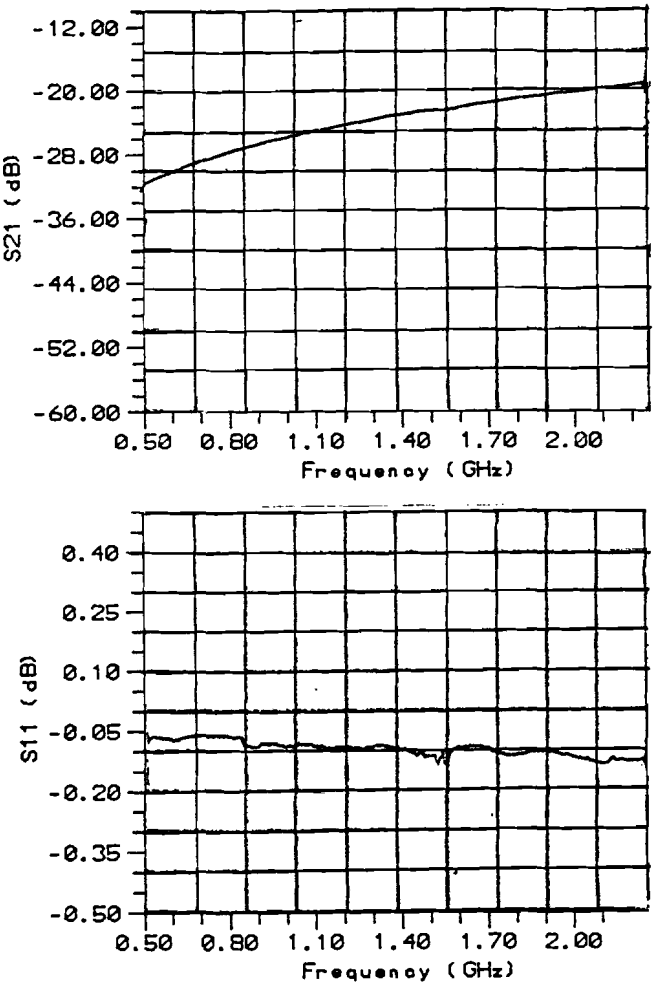

Figure 4.12: Transmission (a) and Reflection (b) Coefficient of Gap-Device

After implementing and verifying the TRL-Calibration the microstrip gap-device is analyzed This gap-device on Epsilam-10 substrate has a gaplength of 0.2 mm. Figure 4.12a shows the transmission coefficient S_{21} of the gap-device.
The measurement is made with a TRL-Calibration between the reference points P3-P4. The transmission of power along the gap increases with frequency. This is due to the fact that the gap impedance, modelled by a capacitance C_g, decreases when the frequency is increased. For the same reason S_{11} (see Figure 4.12b) decreases with frequency. An ideal, lossless device should transmit or reflect all incident signal power:

$$[S_{11}]^2 + [S_{21}]^2 = 1.$$

4.2.5 Simulations

The measured results of the gap-device are compared with simulated results given by the SuperCompact simulation and optimization software. SuperCompact is a software packet with which analysis and synthesis of micowave circuits can be performed. In contrast to a lot of software packets for analysis and synthesis of linear electronic circuits, it can compensate for the propagation effects in a realistic manner. Super-Compact program files consist of different sections:

* Section of variables and constants.
* Section that describes the circuit (by means of nodes)
* Frequency section.(FREQ)
* Output section.(OUT)
* Optimization section.(OPT)
* Data section.(DATA)

Each section begins with its name and ends with an END-statement.

The gap-device is modelled by its equivalent π-circuit of capacitances. The capacitance values are obtained by "running" the optimization procedure of SuperCompact, which uses the measured S-parameters. For this purpose simulation program Circgap.ckt is written (Appendix C). Another simulation program is written using the physical dimensions of the gap: Sgap.ckt (Appendix C). Like this the two different simulations can be compared also. This can give an indication if the π-circuit model of capacitances can be used as en equivalent gap circuit with SuperCompact.

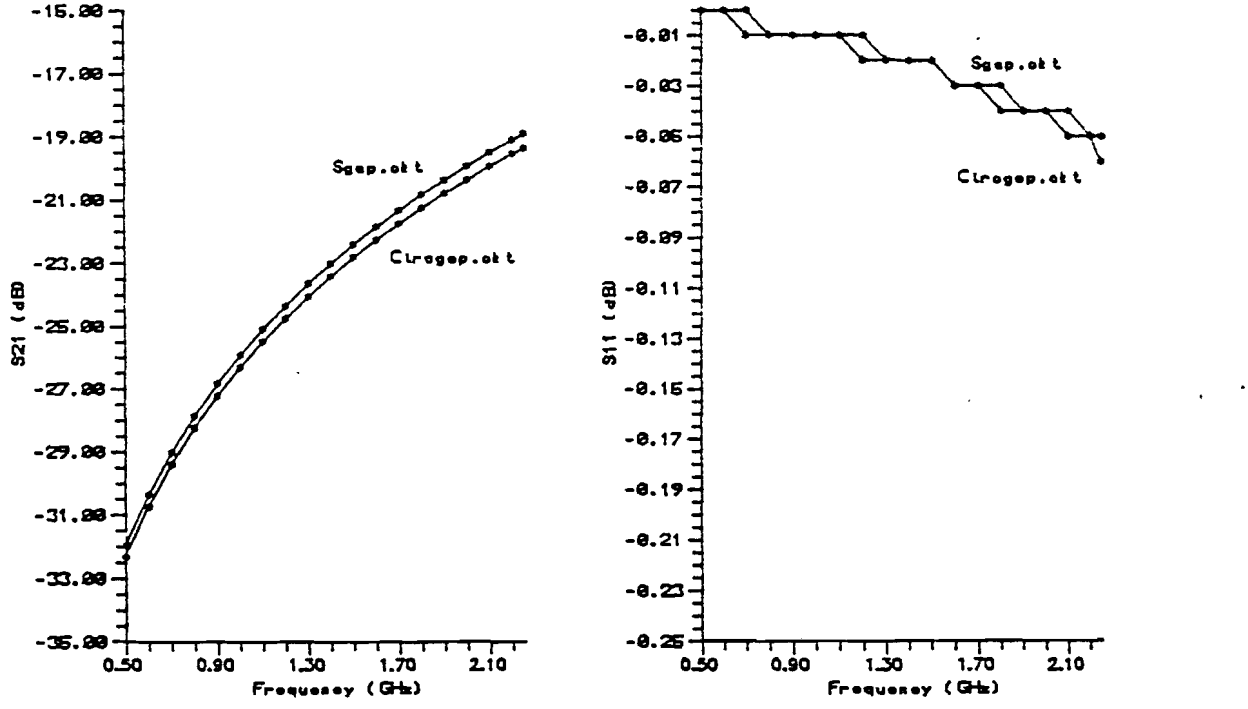

Figure 4.13: Simulated S-parameters of the gap-device

Figure 4.13 shows the results of the two simulations. The simulations show almost exactly the same results. This indicates that the π-model can be used in Super-Compact to model the gap. The simulation software assumes an ideal reciprocal two port network, so $S_{21}=S_{12}$ and $S_{11}=S_{22}$.

The values of the capacitances in the equivalent π-circuit are found by first calculating initial capacitance values, and then using optimization procedures to approximate the measured S-parameters as close as possible. The initial values of the capacitances can be calculated from closed form expressions (Appendix D). The calculated values are:

C_{gi} = 0.087 pF
C_{si} = 0.01 pF

The optimization is done by defining an error function. It expresses the difference between actual responses and the desired responses.

$$e = \frac{1}{m} \sum_{i=1}^{m} k_i \, [e_i]^2 \tag{4.6}$$

By changing the variables the error function is minimized.

This resulted in: C_g = 0.07692 pF
C_s = 0.05572 pF
with an error function: e = 3.3

If we compare the calculated initial values of the gap capacitances with the optimized values of the gap capacitances representing the measured gap, some differences are noticed. The difference between C_{gi} and C_g can be explained by the inaccuracy of the closed form expressions. The accuracy of the closed form expression is given to be within 7%. However the difference between C_{si} and C_s is large.
The reason is that C_s is very sensitive to errors in the physical line lengths. This can be explained by replacing the shunt capacitances C_s in the equivalent gap circuit by their equivalent line lengths l_g. The equivalent line lengths may be calculated as:

$$\Delta l_g = C_s \frac{c \, Z_0}{\sqrt{\epsilon_{re}}} \tag{4.7}$$

An inaccuracy in l_g means an inaccuracy in C_s, so:

$$l_g + \Delta l = (C_s + \Delta C_s) \frac{c\, Z_0}{\sqrt{\epsilon_{reff}}}$$

$$\equiv\equiv\equiv> \quad \Delta l = \Delta C_s \frac{c\, Z_0}{\sqrt{\epsilon_{reff}}} \tag{4.8}$$

If $\Delta l = 0.1\ mm$:

$$\equiv\equiv\equiv> \quad \Delta C_s = 0.018\ pF$$

So C_s= 0.01 pF ± 0.018 pF, in case of a 0.1 mm inaccuracy in linelength. This explains the difference between the calculated C_{si} and the by measurement and optimization obtained C_s.

4.2.5.1 Comparison of measured and simulated results

The simulated and measured results can now be compared. In Figure 4.14 the transmission and reflection coefficient of the gap-devices are visualized.

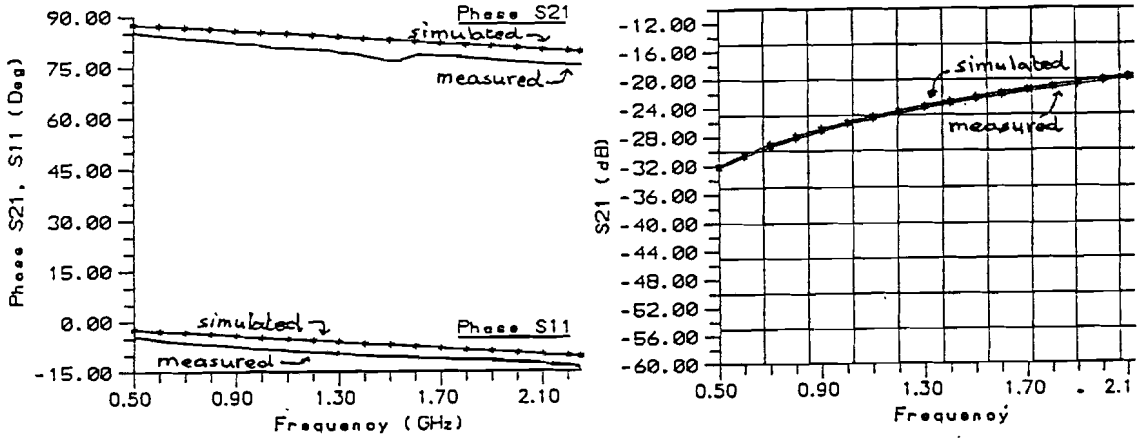

Figure 4.14: Comparison of measured (a) and simulated (b) results

The simulated and measured results in figure 4.14 are in good order. The difference between the phase measurements and simulations is somewhat larger than the differences in magnitude. The phase is very sensitive to changes in line lenghts. For example at 2.25 GHz the phase shift per millimeter transmission line is: ß=7.06°/mm. Because three different standards in different fixtures are used, an inaccuracy in physical dimensions of about 0.1 mm is inevitable. Furthermore there is the inaccuracy in C_s, which can be explained as an incertainty in line-length.

4.2.6 Extension of the TRL-Calibration

An extension of the TRL-calibration experiment to 10 GHz was tried, because of the good results at lower frequency ranges. The same TRL-procedure is followed as for the low-band TRL (0.5-2.25 GHz), with the same standards, on Epsilam-10 substrates.

A TRL-calibration is performed from 2.25-10 GHz using the Line2 Standard. The calibration verification is shown in Figure 4.15. Figure 4.15 makes clear that the accuracy of the calibration at high frequencies decreases. The phase does not show a linear behaviour any more. The insertion phase of the Line2 Standard is still between 20° and 160°. However at the center frequency the difference from the desired 90° phase shift is about 7°.

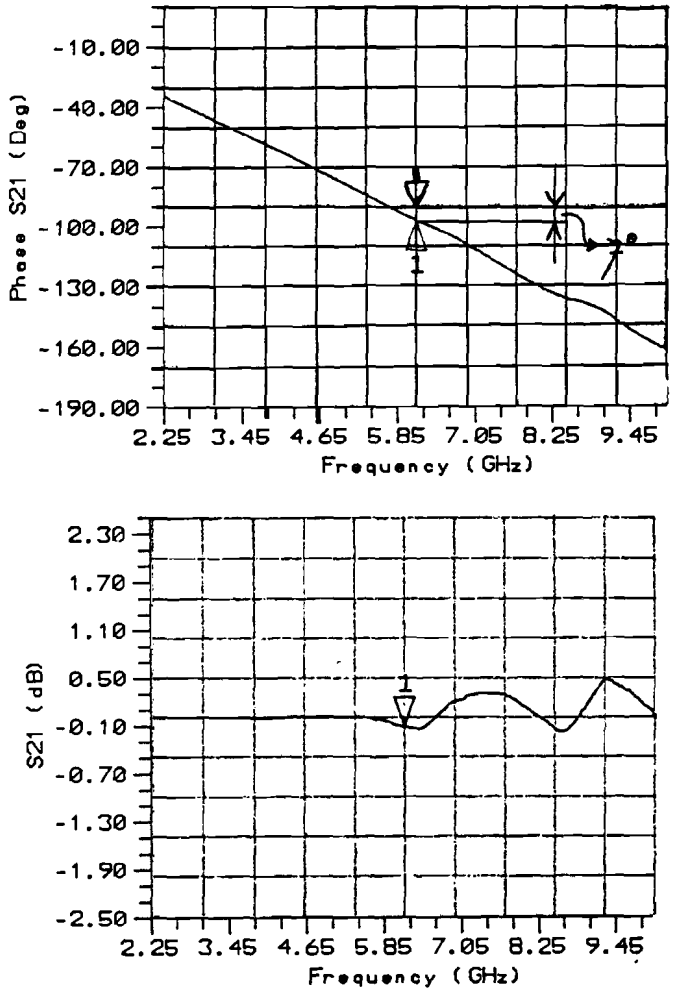

Figure 4.15: Line standard verification measurements

The positive transmission coefficient (at higher frequencies) is due to the inaccuracy of the calibration correction. Transmission lines are passive devices and can not amplify signal power. The curves in figure 4.15 make clear that it is difficult to obtain good calibration accuracy at high frequencies. This is due to the fact that at high frequencies the measurements are more sensitive to imperfect conditions. Deforma-

tion of the coaxial test cables, the use of different fixtures for each standard, incertainty in physical dimensions, the time elapsed between a calibration is effectuated and that it is actually used to do measurements with, are all factors of influence that can not be ignored doing high frequency measurements.

At high frequencies the frequency dependence of the characteristic impedance and the relative permittivity starts to influence the measurements. The standards are fabricated assuming constant characteristic impedance and effective relative permittivity. At 10 GHz also dispersion may have an influence on the measurements.

Figure 4.16 shows the measured S-parameters (TRL-Calibration of 0.5-10 GHz) together with simulations done with the SuperCompact software.

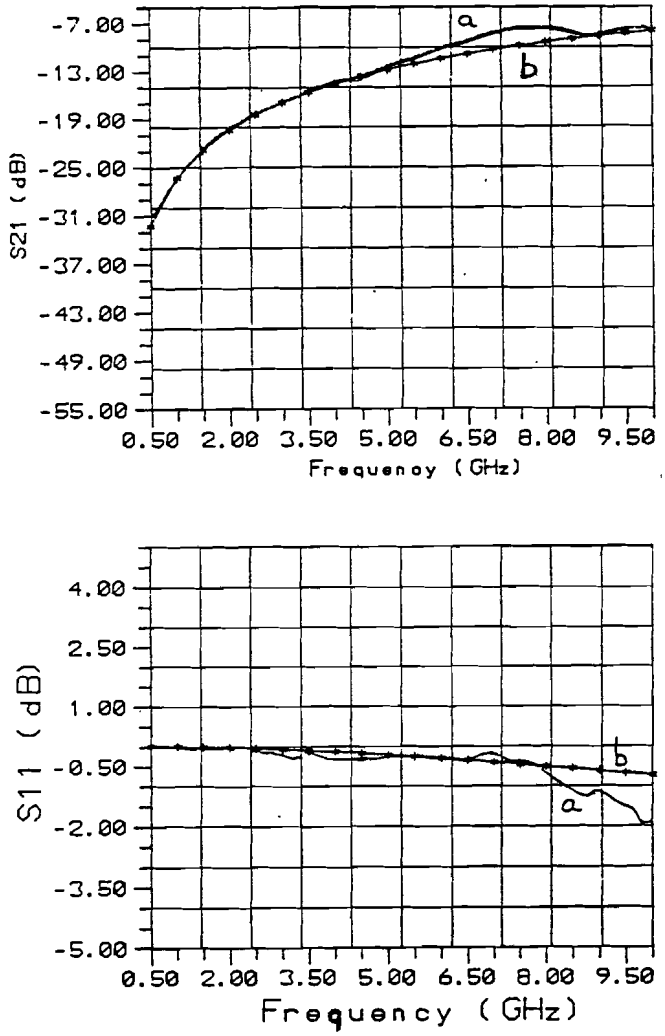

Figure 4.16: Transmission along the gap.
a: measured
b: simulated

4.3 THE Cr:GaAs EXPERIMENT

Besides the Epsilam-10 experiments, I worked on the preparation of the Cr:GaAs experiment. The Cr:GaAs devices, and the fixtures, had to be designed and fabricated. I participated in the part of the fabrication process that was done in the clean room of LEMO. At the beginning of July 1992 the Cr:GaAs devices were ready to be measured. Some measurements, using normal coaxial calibrations, are performed. The results are shown in this paragraph. Also some experimentally derived characteristics of the fixture are presented.
First the layout and the fabrication of the Cr:GaAs devices will be described.

4.3.1 The Cr:GaAs Microstrip and Coplanar Waveguide Gap-Devices

The physical dimensions of the MS and CPW gap devices on the Cr:GaAs substrates were calculated with the software "Lignefen" that is written at LEMO. This software performs a quasi-static analysis using closed form expressions for the characteristic impedance and the effective relative permittivity. The dimensions are calculated to achieve a 50Ω characteristic line impedance. Furthermore some of the physical dimensions can not be changed, for example the substrate height (h). The calculations can be found in Appendix B. The calculated dimensions are:

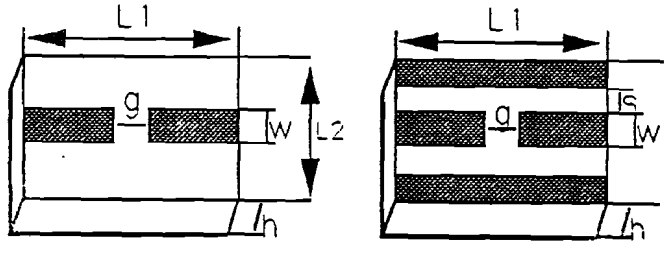

Figure 4.17: Microstrip-and coplanar waveguide device dimensions

g = 5μm - 60μm
h = 0.635 mm
ϵ_r = 13
$\epsilon_{re(CPW)}$ = 6.5
$\epsilon_{re(MS)}$ = 8.4
L1 = 5 mm
L2 = 5 mm
W = 0.43 mm
S = 0.26 mm (CPW-case)

The stripwidth of the central stripconductor W is calculated as 430 μm. To measure the characteristics of the devices, they have to be mounted into a fixture. The fixture makes the transition between the planar transmission line technology and the measurement equipment, that uses coaxial lines, possible. However the calculated central strip width of 430 μm is too small to connect to the microstrip-to-coax launch directly. So "transition components" are needed.

Since the stripwidth of the transition components does not differ a much from the stripwidth of the Cr:GaAs devices, it would have been possible to enlarge the stripwidth by means of "tapering". With this technique the stripwidth is enlarged by a number of small steps. The characterisitc impedance is not changed. Because at LEMO there was already decided to do it with other transition components, I did not investigate the possibilities of tapering any further.
The transition components are made on Alumine substrates (Al_2O_3), with gold metallization. They have the same layout as the Cr:GaAs device, but with larger

dimensions. The central strip width of W = 0.69 mm is large enough to make a connection with the microstrip-to-coax launch possible. The calculations can be found in Appendix B.

The layout of the Cr:GaAs MS and CPW devices connected with bonding wires to the transition components on Al_2O_3 substrate, is illustrated in Figure 4.18. The spacing between the Cr:GaAs device and the transition components is in reality as small as possible.

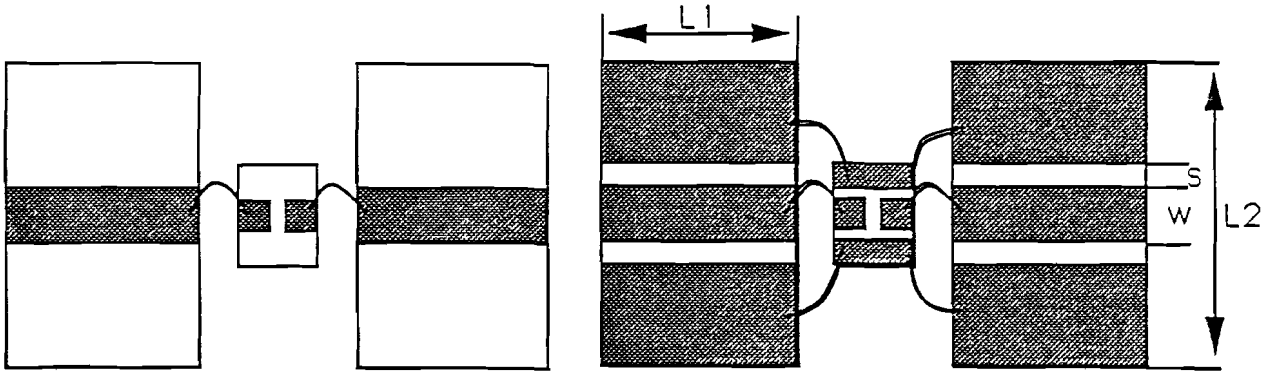

Figure 4.18: Layout of Cr:GaAs MS and CPW devices connected to transition components.

L_1 = 22.5 mm W = 0.69 mm
L_2 = 50 mm S = 0.26 mm
ϵ_r = 10 h = 0.635 mm
$\epsilon_{re(MS)}$ = 6.8 $\epsilon_{re(CPW)}$ = 4.25

The transition components are glued in metal (MS case) or plexiglass (CPW case) boxes. To assure good contacts between the box with the connectors and the transition components we use silverpaint. Especially the connection of the central conductor strip of the transition component with the connector in the box, is a very precise work. It has to be done with a microscope.
The box with the transition components represent the fixture of the Cr:GaAs device. The gap-device is placed between two transition parts. Bonding wires connect the metallized strips of the transition components with the equivalent parts of the gap-device. The final gap-device in fixture will be:

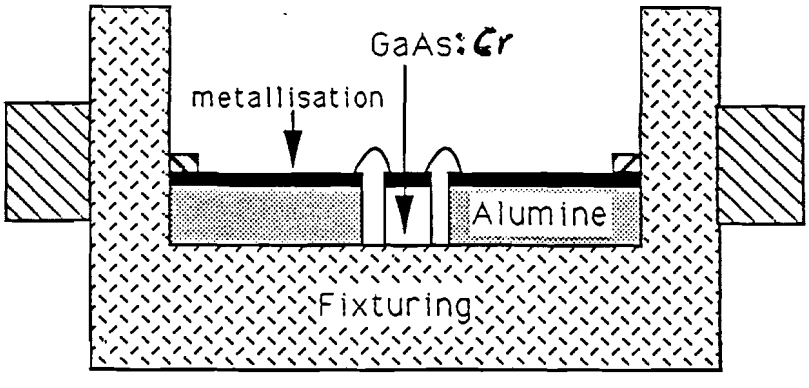

Figure 4.19: Cr:GaAs device in fixture

In this figure, only six bonding wires are designed, while in reality more bonding wires are connected to make a better signal transmission possible.

The gap-devices on the Cr:GaAs substrates are realized partially in the clean room at LEMO, partially in other laboratories in France. The transition components are fabricated at CIME (Centre Interuniversitaire du Micro-Electronique), another laboratory of INPG in Grenoble.

4.3.2 Fabrication Process

The fabrication of the microstrip and coplanar waveguide devices is done partially at LEMO and partially at other laboratories. In total five different laboratories in four different cities in France were involved in the fabrication process.

The used substrate is chromium doped gallium arsenide (Cr:GaAs). The metallization layer deposited on the substrate must possess some specific characteristics, like:

* low resistivity (low ohmic losses)
* good resolution
* oxidation resisted
* good fixation to the substrate

Normally all good conductors (silver, copper, aluminium) can be used. However with some substrates (e.g. ceramics) the fixation is not good enough. In this case, an extra, very thin intermediate layer has to be adjusted, which is less conductive but sticks better to the substrate. Normally a layer of an alloy is used for this purpose. The metallization structure is deposited on the substrate using a mask. The mask is designed at LEMO, but fabricated on glass at a company (at Besançon).

To transfer the pattern on the mask to the substrate-wafer, we used two slightly different photolithographic methods:

1) Stripping Technique
2) Lift-Off Technique

With the stripping technique the wafer surface is completely metallized with aluminium. Then a second layer of thin photosensitive material, the resist, is put on. This is done by centrifugation. The mask pattern is transferred to the wafer by a lithographic exposure tool.

After illumination of the wafer, we eliminate either the part of the resist that is exposed to the light (positive photoresist) or the other part (negative resist) with a chemical solution. The free metallization can now be dissolved with an acid solution. After that the remaining photoresist can be dissolved. The process is visualized in Figure 4.20.

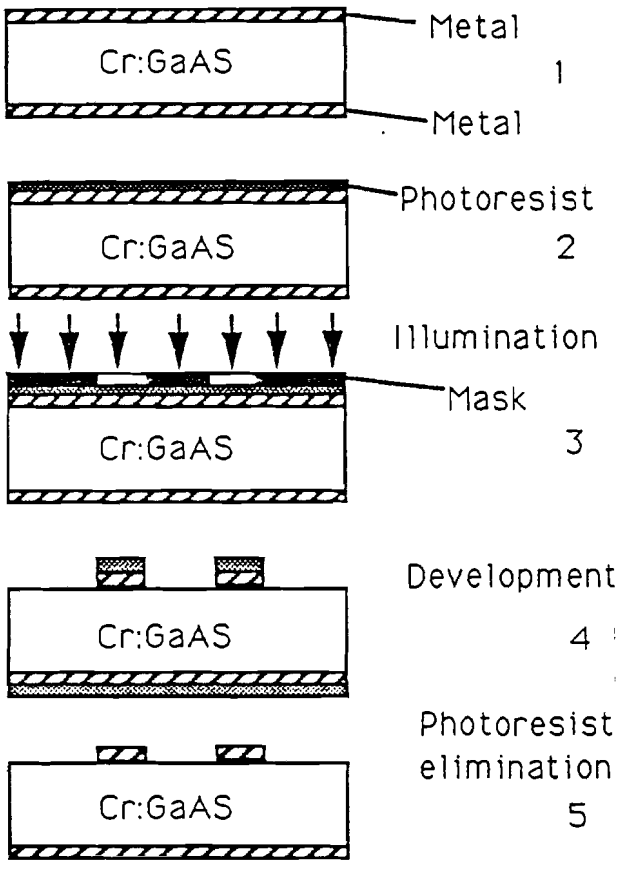

Figure 4.20: The stripping technique: Photolithographic etching process for microstrips and coplanar waveguides.

The lithographic exposure tool illuminates the wafer through the mask. Like this the mask pattern is printed in the resist layer. The most important performance parameter of the photolithographic exposure tool is its resolution. The resolution is the minimum feature dimension that can be transferred with high fidelity to the wafer.

We used the method of contact printing, where the mask is pressed to the wafer. This technique provides a very high resolution ($\sim 1\mu m$), but suffers from possible damage to the wafer caused by dust particles between the mask and the wafer. Thus, the repeatability of the operation is not very high, and the lifetime of the mask not very long.

Because the GaAs technology is very delicate and not yet practiced much at LEMO we encountered some serious problems. It took a lot of time and delay to fabricate a wafer with good components.

Some of the problems were:

- Metallization that did not stick to the substrate.
- The acid dissolver used to remove the free metallization (step 4 Fig. 4.20) also attacked the Cr:GaAs substrate surface.

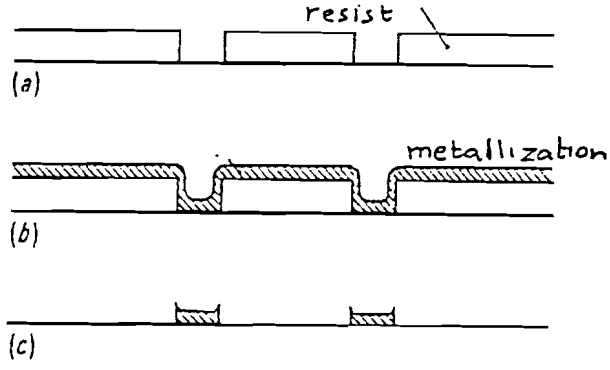

Figure 4.21: The Lift-Off Technique

To avoid these problems we tried the Lift-Off technique. The difference with the stripping method is that the resist layer is put on the wafer before the metallization. Also illumination with the mask is done before metallization (Figure 4.21).
The remaining photoresist with the metallization on it is then dissolved.
This method has the advantage that we do not need to dissolve the metallization with a chemical acid solution that also attacks the substrate surface.

To avoid also the problem of the bad fixation, one wafer was sent to a laboratory of ECL (Ecole Centrale de Lyon). There, a thin alloy metallization was put on the wafer, which makes good contacts between the wafer and the alluminium metallization possible. This last method resulted in one wafer with good components at the end of May 1992.

To perform measurements, the devices on the wafer still had to be cut and mounted into a fixture. This last step in the fabrication process also took some time. Finally, the wafer was cut at CSF Thomson in Paris. The packaging of the devices in their fixture and the connection of the bonding wires to the Al_2O_3 transition components was done at CIME. At the beginning of July 1992 the first measurements with the gap devices were made.

4.3.3 Verification Measurements

Before the measurements with the gap-devices are made, some measurements with the fixture (box with transition components) are performed. It is very important to know the characteristics of the fixture (e.g. the characteristic impedance), to make a good interpretation of the measured results possible.

A TDR measurement of a continuous CPW Through Line on alumine substrate in the fixture is performed. The result is shown in grafic 4.22. In the upper graphic, the input step, the transition discontinuities can be seen clearly. In the lower graphic the scale is changed to see the discontinuities better.

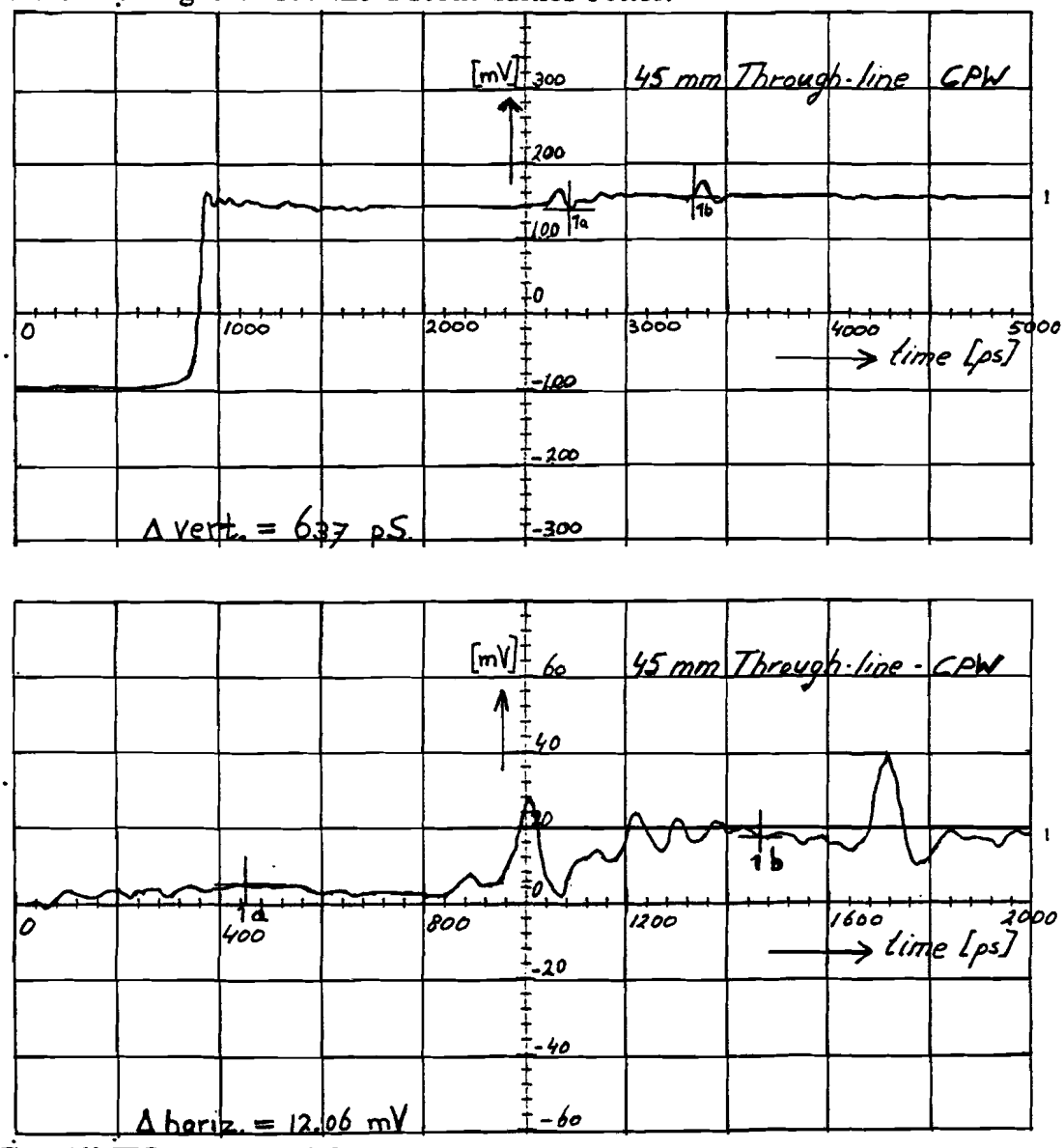

Figure 4.22: TDR measurement of 45 mm continuous transmission line on Al_2O_3 substrate.

The characteristic impedance of the transmission line can be calculated as:

E_r= 12.06 mV, E_i=250 mV
==> Reflection Coeffiecient $|\Gamma|$ = 12.06/250 = 0.048
==> SWR = 1.048/0.952 = 1.1
==> Z_c = 50*SWR = 55 Ω

There will be a slight mismatch between the characteristic impedances of the test cables, the transition components and the Cr:GaAs devices. Also from Figure 4.22 we can see that the elapsed time between the two pulses of the two connector discontinuities, $t_0 \approx$ 640 ps. This corresponds with a frequency of resonance of:
$F_{res} = 1/t_0 \approx$ 1.6 GHz.

The frequency of resonance can be derived theoretically by:

$$L_{res} = n \cdot \frac{\lambda}{2}, \qquad \lambda_n = \frac{v_{pn}}{f_{resn}}$$

$$\frac{f_{resn}}{n} = \frac{c}{2L_{res}\sqrt{\epsilon_{re}}} \tag{4.9}$$

With the in Appendix B calculated effective relative permittivity, ϵ_{re}= 4.25 and L = 45 mm, we obtain:

$$f_{res} = 1.62 \text{ GHz}$$

This corresponds well with the TDR results. In Figure 4.23 the reflection of the 45 mm continuous transmission line is measured with the VNA.

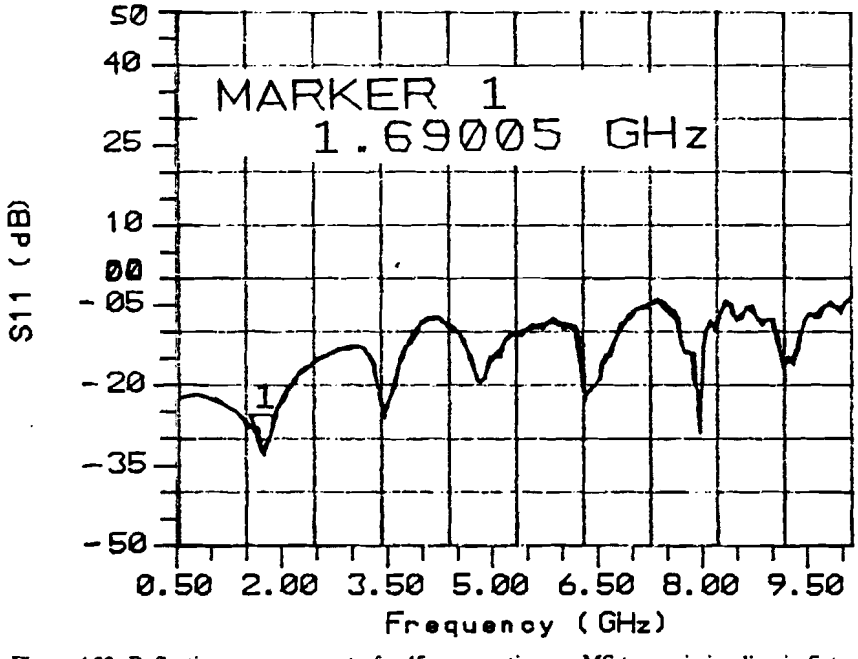

Figure 4.23: Reflection measurement of a 45 mm continuous MS transmission line in fixture

Figure 4.23 shows the same resonances in the frequency domain. The height of these resonaces depends on the "strength" of the discontinuities at the ends of the transmission line. These discontinuities are due to mismatches between characteristic impedances of the CPW transmission line and the coaxial test cables and non-ideal silver-paint connections.

4.3.4 Cr:GaAs microstrip gap-device measurement:

In July 1992, we could measure a Cr:GaAs gap device. We used a normal coaxial calibration. In Figure 4.24 the transmission and reflection coefficient of a microstrip device with a gap of 60 μm is shown. The reflection is over the whole frequency range of 0.5 - 10 GHz better than 2 dB, which is good.

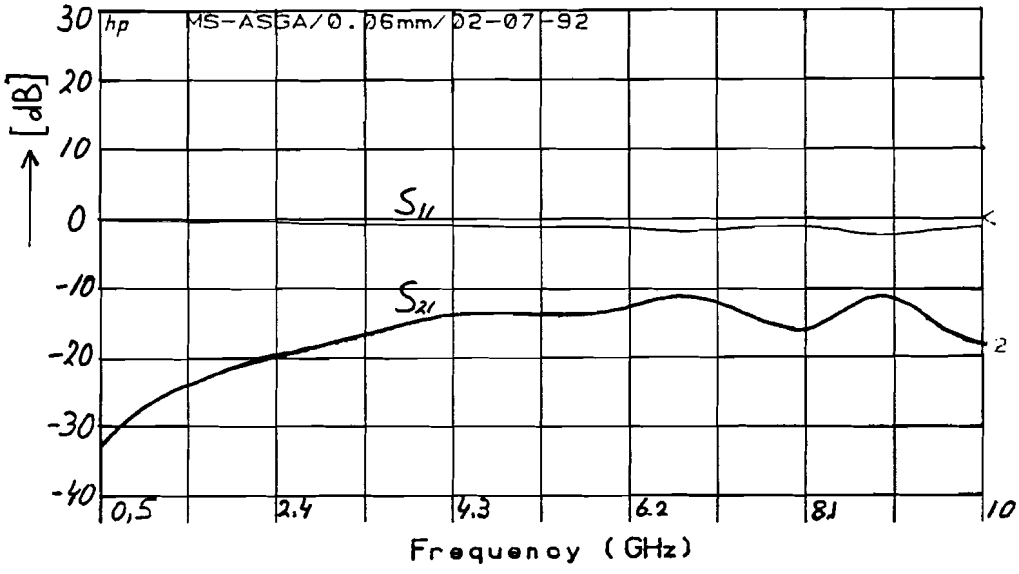

Figure 4.24: Reflection and transmission coefficient measurement of a Cr:GaAs MS gap device.

In Figure 4.25 three different gap-device measurements are shown. This figure shows that the measurement with the Cr:GaAs device has two peaks at about 7 and 9 GHz. This is probably due to the bonding wires. The bonding wires can be represented by an inductance, and may introduce the resonances. Figure 4.25 also shows that the transmission coefficient S_{21} of the Cr:GaAs devices is smaller than the S_{21} of the Epsilam-10 devices while the Cr:GaAs device has a smaller gaplength. This must be due to the complex fixturing with the bonding wires.

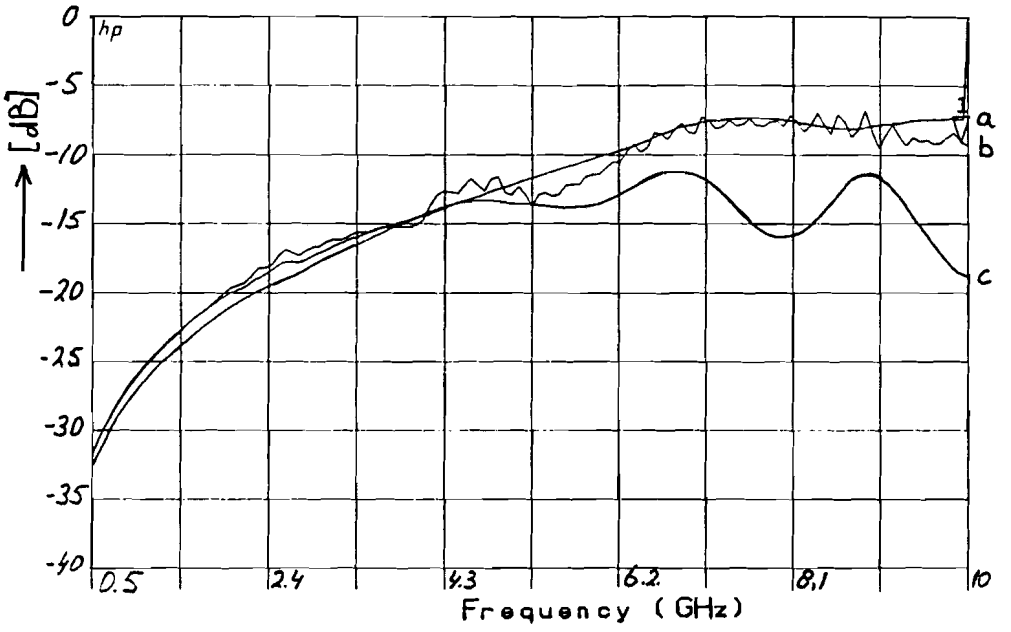

Figure 4.25: MS gap devices transmission measurements:
a: TRL Epsilam-10 MS gap device, g=200μm
b: Coax Cal. Epsilam-10 MS gap device, g=200μm
c: Coax Cal. Cr:GaAs MS gap device, g=60μm.

CONCLUSIONS AND RECOMMENDATIONS

The objective of my graduation work was the characterization of optoelectronic microwave switches on Cr:GaAs substrates. Because the realization of the devices on Cr:GaAs substrate had a lot of delay, this could be done only in the "off"-state, without illumination.

Microstrip devices on Epsilam-10 substrates are designed and realized to test the characterization methods. Epsilam-10 has a high relative permittivity (ϵ_r = 10) like Cr:GaAs and therefore approximates the behaviour of Cr:GaAs upto frequencies of about 10GHz.

The realized Epsilam-10 devices have to be mounted into fixtures. The fixtures change the Reference Plane of the measurements and thus the measured S-parameters. To obtain the characteristics of the DUT, different de-embedding methods can be used. We compared the TRL-Calibration method, a one-tier de-embedding method, with normal coaxial calibration, where two-tier de-embedding is needed. The measurements are compared with simulations. The simulations are done with Super-Compact.

The TRL-Calibration method is one of the most popular in-fixture calibration methods. It shows clear advantages over the basic TSD method, like simple realizable stan- dards. TRL measurements give the corrected DUT parameters directly. With coaxial calibrations the DUT characteristics have to be de-embedded from the overall measured characteristics. For this purpose an equivalent circuit for the fixture is used. This decreases the accuracy of the obtained results, which is a great disadvantage of two-tier de-embedding.

The Figures in Chapter 4 show that a TRL implementation for the frequency band 0.5-2.25 GHz is very well possible. The extension of the TRL-implementation to higher frequencies shows that the influence of the measurement environment on the accuracy increases. However, even with different fixtures for all the standards, the measurement accuracy is still acceptable. Even in the frequency range of 0.5-10 GHz the measured S-parameters are in good order with the simulations.

However, the implementation of TRL-Calibrations becomes more and more delicate. At high frequencies it is advisable to use one shiftable fixture for all standards, to maintain the physical measurement environment as good as possible.

A disadvantage of calibrations in general is their sensitivity to changes in the measurement environment. Therefore the fixture should be realized with great care, and should be kept as simple as possible.

The influence of the fixture on the measurements is clear with the Cr:GaAs device measurements. The measurements done with a microstrip gap-device on Cr:GaAs substrate show the same behaviour as the gap-devices on Epsilam-10. The influence of the bonding wires on the measurements is very clear. The exact influence of the bonding wires must still be examined. Maybe it will be better to make a fixture that does not use bonding wires. Tapering could be a solution.

The influence of a non-constant environment, that cannot be corrected for, is minimized by performing on-wafer measurements. On-wafer measurements can provide very precise information about the intrinsic DUT parameters. To perform on-wafer measurements special, expensive equipment is needed. Performing on-wafer measurements, probe-tips are pushed on the planar conductors with the aid of a microscope. Special probes for microstrip and coplanar waveguide devices are commercially available. Also wafers with transmission line standards are commercially available, so they do not have to be realized specially. With on-wafer measurements the DUT can be characterized before the wafer is cut and before the devices are packaged. This has the advantage that bad devices can already be discovered before packaging.

At LEMO the on-wafer measurement equipment is already available. With the special probes the gap-devices on the Cr:GaAs wafer could be characterized relatively simple and fast. Because the GaAs technology is very delicate, and not much experienced at LEMO, the fabrication of the Cr:GaAs devices took more time than expected. Performing on-wafer measurements might be a solution to obtain very quick, very accurate measurement results of the gap devices on Cr:GaAs substrates.

EPILOGUE

From December 1991 to July 1992 I performed the graduation work for my Master Thesis at the Laboratoire d'Electromagnétisme, Micro-ondes et Opto-électronique (LEMO) of the Institut National Polytechnique de Grenoble (INPG) in France.

Doing my graduation work at a foreign university offered me some great opportunities. Above all the international aspect was very important to me. Grenoble is a town with 45.000 students of which 5.000 foreign european students. At LEMO I worked with students from all of Europe, Northern Africa and the Far East. Working in such a multinational environment, where you meet people looking at things in a very different way, handling and discussing problems in other ways also, has certainly widened my view.

Although France may be not very far from The Netherlands, there are big differences in culture and in the way things are organized at work. I can not say this was always easy, but it sure had a stimulating influence on my graduation work and was an interesting experience.

Doing a master thesis at a foreign university can be very advantageous, both to the student and the universities, when good agreements about the subject of the thesis and the organization of the work are made.

To me it has been a very unique and learning experience. I would like to thank Prof.Dr.ir. G. Brussaard very much, for letting me take the opportunity of doing my graduation work at LEMO.

Bas Slotboom

LITERATURE

[1] Platte,W.--Optoelectronic Microwave Switching--IEE Proc., Vol.132, Pt.J, No.2, April 1985.

[2] Lee,C.H.--Picosecond Optics and Microwave Technology-- IEEE Trans. Microwave Theory and Techniques, Vol.38, No.5, 1990.

[3] Johnson,A.M. and Auston,D.H.--Microwave Switching by Picosecond Photoconductivity--IEEE J. Quantum Electronics, Vol.QE-11, No.6, 1975.

[4] Simons,R.--Optical Control of Microwave Devices--Artech House, Boston, London, 1990.

[5] Lee,C.H.--Picosecond optoelectronic switching in GaAs--Appl.Phys.L., Vol.30, No.2, 1977.

[6] Seeds,A.J. and Salles de,A.A.--Optical control of microwave semiconductor devices--IEEE Trans. Microwave Theory and Techniques, Vol.38, No.5, 1990.

[7] Lee,C.H.--Picosecond optoelectronics and millimeter-wave technology--M6.1,p.-61,1988.

[8] Sze,S.M.--Semiconductor Devices, Physics and Technology--New York--John Wiley&Sons--U.S.A.--1985.

[9] Gupta,K.C.,Garg,R.,Bahl,I.J.--Microstrip Lines and Slot Lines--Dedham,MA--Artech House--1979.

[10] Kumar,D. et al.--A study of gaps in microstrip transmission lines--Int.J.Electronics--Vol.41--No.6--p.617-620--1976.

[11] Elmore,G.E. and Salz,L.J.--Quality microwave measurement of packaged active devices--Hewlett Packard J.--Vol.38--p.39-48--1987.

[12] Hewlett Packard--Applying the HP8510 TRL Calibration for non coaxial measurements--Product Note 8510-8--1987.

[13] Simons,R.N. and Ponchak,G.E.--Modeling of Some Coplanar Waveguide Discontinuities--IEEE Trans.Microw.T.Techn.--Vol.36--No.12--1988.

[14] Franzen,N.R. and Speciale,R.A.--A new procedure for system calibration and error removal in automated S-parameter measurements--European Microw. Symp.Dig.--p.69-73--1975.

[15] Lane,R.--Deembedding Device Scattering Parameters--Microw.J.--Vol.27--p.149-156--August 1984.

[16] Gardiol,F.--Conception et réalisation de circuits microrubans--Ann.Télécommun.--Vol.43--No.5,6--p.220-236--1988.

[17] Engen,G.F. and Hoer,C.A.--Thru-Line-Reflect: An improved technique for calibrating the dual six portautomatic network analyzer--IEEE Trans.Microw. T.Techn.--Vol.27--No.12--p.987-993--1979.

[18] Souza,J.R. et al.--S-parameter characterisation of coaxial to microstrip transition--IEE Proc.--Vol.129--Pt.H--No.1--p.37-40--1982.
[19] Fitzpatrick,J.--Error models for systems measurement--Microwave J.--p.63-66--May 1978.
[20] Wen,C.P.--Coplanar Waveguide: A surface strip transmission line suitable for nonreciprocal gyromagnetic device applications--IEEE Trans. Microwave T. Theory--Vol.17--p.1087-1090--1969.
[21] Benedek,P.and Silvester,P.--Equivalent capacitances for microstrip gaps and steps--IEEE Trans.Microwave T.Theory--Vol.20--p.729-733--1972.
[22] Meada,M.--An Analysis of Gap in Microstrip Transmission Lines--MTT 20--No.6--1972.
[23] Gopinath,A. and Gupta,C.--Capacitance parameters of discontinuities in microstrip lines--IEEE Trans.Microwave T.Theory--Vol.26--p.831-836--1978.
[24] Getsinger,W.J.--Microstrip Dispersion Model--IEEE Trans.Microwave T.Theory--Vol.21--p.34-39--1973.
[25] Travaux Pratiques 3ème année (TP.332)--Etude de lignes d'interconnexion pour circuits sub-nanosecondes par réflectométrie temporelle--ENSERG--LHOG.
[26] Angénieux,G.--Caractérisation électromagnétique de connexion pour circuits logiques rapides: outils d'analyse théorique et expérimentale--Thèse de doctorat d'etat--USMG--INPG--Octobre 1987.
[27] Moffitt,L.R.--Time-Domain Reflectometry Theory and Applications--Aplication Note 75--p.3-8--Hewlett Packard.
[28] Travaux Pratiques 3ème année (TP.335)--Evaluation expérimentale de dispositif micro-ondes par analyse vectorielle de réseaux--ENSERG--LHOG
[29] Wiltron--Information Technique--Quelques regles pour éviter les erreurs de mesure--Wiltron Company--Mountain View--USA.
[30] Mabrouk,M.--Caractérisation de lignes monolithiques sur GaAs pour circuits microondes--Thèse de doctorat d'etat--LEMO--INPG--juillet 1991.

APPENDIX A

MICROSTRIP AND CPW STRUCTURES

A.1 MICROSTRIP

The microstrip is made of a thin substrate with a conducting strip on top. The bottom side is totally metallized, forming a groundplane (See Figure A.1). Microstrip lines are transmission lines that are used extensively in microwave integrated circuits (MICs), because of their planar configuration. The open top structure of microstrips makes it very easy to mount active or passive devices into their structure. However due to the presence of the dielectric-air interface a TEM-mode of propagation is not possible. This can be made clear with the aid of the Maxwell equations and the assumption of quasi-static field distribution (see Figure A.1).

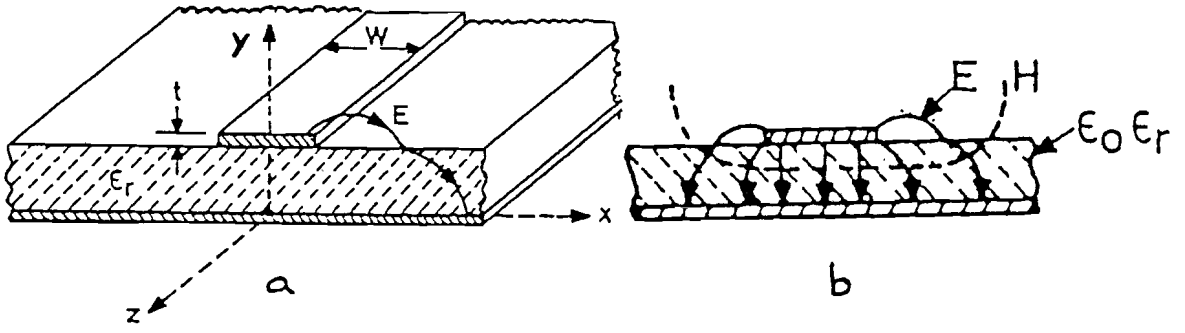

Figure A.1: a) Microstrip Configuration b) Electromagnetic field distribution

$$H_x|_d = H_x|_a$$

Using MAXWELL's equations:

$$\Delta \times \underline{E} = -\frac{\partial \underline{B}}{\partial t}$$

$$\underline{B} = \mu \underline{H}$$

We may write: $(\Delta \times E)_x|_d = \mu_r (\Delta \times E)_x|_a$

$$\mu_r \frac{\partial E_z}{\partial y}|_a - \frac{\partial |E_z}{\partial y}|_d = (\mu_r - 1) \frac{\partial E_y}{\partial z} \qquad (A.1)$$

In these equations subscript "a" stands for air and subscript "d" for dielectric.

Since $\mu_r <> 1$ and $E_y <> 0$ this expression implies that $E_z <> 0$. In a similar way it can be shown that $H_z <> 0$. So the mode of propagation is not purely TEM.

It may be pointed out that it is only the E_x and H_x at the dielectric-air interface that lead to the non-TEM nature of the microstrip structure. Since these effects are much smaller than the main field most of the energy is transported in the transversal mode. There is only a slight difference from the TEM-mode and thus the propagation mode in microstrip is considered to be quasi-TEM.

In this quasi-TEM mode the inhomogeneous microstrip structure is replaced by an equivalent structure where the conductors (strip and ground) have the same dimensions but are in a homogeneous surrounding with an effective relative permittivity ϵ_{re}. The value of ϵ_{re} is derived from the static capacitance of the inhomogeneous structure as: [16]

$$\epsilon_{re} = \frac{\epsilon_r + 1}{2} + \frac{\epsilon_r - 1}{2} \left(1 + 10 \frac{h}{W}\right)^{-ab} \qquad (A.2)$$

$$a = 1 + \frac{1}{49} \ln\left(\frac{(w/h)^4 + (w/52h)^2}{(w/h)^4 + 0.432}\right) + \frac{1}{18.7} \ln\left(1 + \left(\frac{w}{18.1h}\right)^3\right)$$

$$b = \left(\frac{\epsilon_r - 0.9}{\epsilon_r + 3}\right)^{0.053}$$

If frequency increases the electromagnetic field concentrates in the center of the substrate. This increases the effective relative permittivity. To take this dispersive effect into account the static permittivity is replaced by a frequency dependent

function [24].

$$\epsilon_{re}(f) \approx \epsilon_r - \left(\frac{\epsilon_r - \epsilon_{re}}{1 + G\,(f/f_d)^2}\right) \qquad (A.3)$$

$$f_d = \frac{Z_c}{2\mu_0 h} \quad Hz \qquad \textit{:Dispersion frequency}$$

$$G = 0.6 + 0.009\,Z_c \quad \Omega$$

From this equation it can be seen that if $f < f_d$ the dispersion does not have to be taken int account.

Microstrip lines have been studied using quasi-static approximations as well as fullwave analysis. Fullwave analysis provides information regarding frequency dependence of the phase velocity (v_p) and the characteristic impedance (Z_c). However fullwave analysis uses numerical methods which involves extensive computations. For easy design of microstrip circuits closed form expressions are used. The equations used to design our components are all based on the quasi-static analysis and can be found in [9]. Results in literature indicate that at the frequency band uptill 10 GHz dispersion is negligible and the quasi TEM analysis may be used.

A.2 COPLANAR WAVEGUIDE (CPW)

The coplanar waveguide (CPW) structure was first proposed by Wen in 1969 [20]. A coplanar waveguide consist of a center strip conductor and two semi-infinite ground planes on either sides of it superimposed on a dielectric substrate. Like the microstrip structure also coplanar waveguide is a planar structure and therefore very convenient to use in MIC's. Since coplanar waveguide also has an open top structure its propagation mode is not pure TEM. Although the electromagnetic field distribution is different from the electromagnetic field distribution in microstrip, the problem can be handled in a similar way. We may thus consider the mode of propagation quasi-TEM. The electric and magnetic field distribution is shown in Figure A.2.

coplanar waveguide offers some advantages over conventional microstrip, like:

Mounting of lumped components in shunt or series configuration is easy, drilling wrap-around or via holes through the substrate is not needed.

The electromagnetic field in the substrate is relatively small and therefore the dielectric losses are small too.

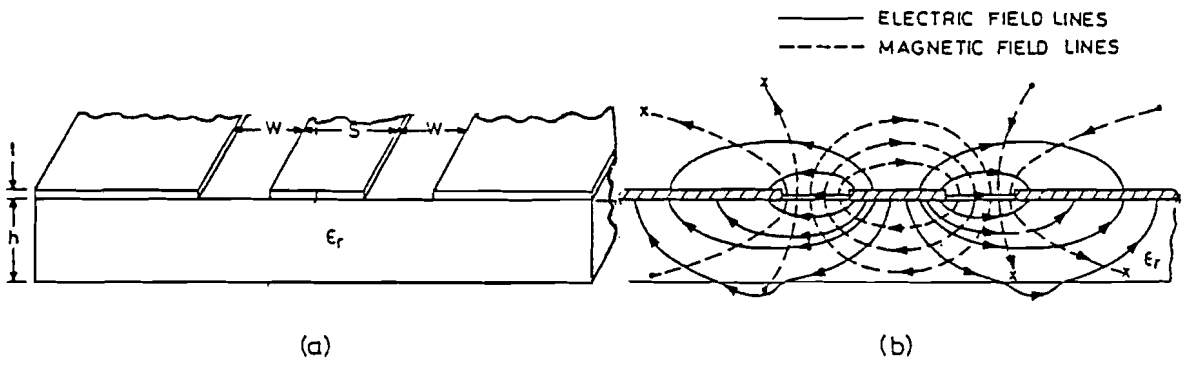

Figure A.2: Electric and magnetic field distribution in coplanar waveguide

One of the problems of the coplanar waveguide is heat removal from the device. It is difficult to provide an efficient heat sink without perturbing the electromagnetic field in the coplanar waveguide. An additional groundplane on the other side of the three conductors is sometimes used.

Like microstrip, coplanar waveguide can be described using closed form expressions as well as full wave analysis. For the design of our devices we used the closed form expressions as given in [9] for coplanar waveguide.

APPENDIX B

Microstrip And CPW Design Equations

B.1 INTRODUCTION

For optimization and computer-aided-design of microstrip and CPW circuits simple closed form expressions are needed. The fullwave analysis who takes into account the time variations of the electric and magnetic fields in the microstrip or CPW involves extensive computations. Furthermore the results from different publications indicate that the quasi-TEM analysis may be used below X-band frequencies. The quasi-TEM analysis uses closed form expressions for the characteristic impedance (Z_c) and the effective dielectric constant (ϵ_{re}). These design equations can be found in: "Microstrip Lines and Slotlines" by Gupta, Garg and Bahl [9].

B.2 MICROSTRIP DESIGN EQUATIONS

$$Z_c = \frac{120\pi}{2\pi\sqrt{\epsilon_{re}}} Ln\left(8\frac{h}{W} + 0.25\frac{W}{h}\right) \qquad \left(\frac{W}{h} \leq 1\right) \tag{B.1}$$

$$Z_c = \frac{120\pi}{\sqrt{\epsilon_{re}}} \left\{\frac{W}{h} + 1.393 + 0.667\, Ln\left(\frac{W}{h} + 1.444\right)\right\}^{-1} \qquad \left(\frac{W}{h} \geq 1\right) \tag{B.2}$$

$$\epsilon_{re} = \frac{\epsilon_r + 1}{2} + \frac{\epsilon_r - 1}{2} F(W/h) \tag{B.3}$$

The maximum relative error in ϵ_{re} and Z_c is less than 1 percent.
W: Width of the central strip.

$$F(W/h) = (1 + 12\frac{h}{W})^{-\frac{1}{2}} + 0.04(1 - \frac{W}{h})^2 \qquad (\frac{W}{h} \leq 1)$$

$$F(W/h) = (1 + 12\frac{h}{W})^{-\frac{1}{2}} \qquad (\frac{W}{h} \geq 1)$$

B.3 COPLANAR WAVEGUIDE DESIGN EQUATIONS

$$Z_c = \frac{30\pi}{\sqrt{\epsilon_{re}}} \frac{K'(k)}{K(k)}, \qquad k = \frac{W}{W + 2S} \tag{B.4}$$

$$\frac{K'(k)}{K(k)} = \frac{1}{\pi} Ln \{ 2 \frac{1 + \sqrt{k}}{1 - \sqrt{k}} \} \qquad (0.707 \leq k \leq 1)$$

$$= \frac{\pi}{Ln \{ 2 \frac{1 + \sqrt{k}}{1 - \sqrt{k}} \}} \qquad (0 \leq k \leq 0.707)$$

$$\epsilon_{re} = \frac{\epsilon_r + 1}{2} \{ \tanh (1.785 \, Log \frac{h}{S} + 1.75) + \frac{kS}{h} \{(0.04 - 0.7k + 0.01 (1 - 0.1\epsilon_r)(0.25 + k)\} \} \tag{B.5}$$

S: Spacing between central strip and the groundplanes on either side of the conducting central strip.

B.4 CALCULATED Cr:GaAs DEVICE DIMENSIONS AND CHARACTERISTICS

For both the microstrip and coplanar waveguide devices on the Cr:GaAs substrate the fixed dimensions are:

h = 0.635 mm
t = 10 μm : thickness of metallization.
and: $\epsilon_r = 13$

We want to have a characteristic impedance of $Z_c = 50\Omega$. In the microstrip case this can be done by varying W. In the coplanar waveguide case both W and S can be changed to obtain $Z_c = 50\Omega$. With simulation software, based on the above given equations, the following physical dimensions for our devices on Cr:GaAs substrates were found:

W = 0.43 mm
S = 0.26 mm (only for CPW)

For reasons of easy mask design the central strip width W is chosen to be the same for microstrip and coplanar waveguide. These dimensions result in a characteristic impedance and effective relative permittivity of:

Z_c= 51.3 Ω, ϵ_{re}= 8.4 for the microstrip devices on Cr:GaAs substrates.
Z_c= 49.8 Ω, ϵ_{re}= 6.5 for coplanar waveguide devices on Cr:GaAs substrates.

B.5 CALCULATED DIMENSIONS OF TRANSITION COMPONENTS

The transition components are fabricated on Al_2O_3. It is a ceramic material with very low losses. it is a very hard material that can break easily. The fixed dimensions are:

h = 0.635 mm
t = 10 μm
ϵ_r = 10

The calculated dimensions are:

In CPW case: W = 0.69 mm, and S = 0.26 mm.
In MS case: W = 0.69 mm

This results in: Z_c= 54Ω, ϵ_{re}= 4.25 in the CPW case.
Z_c= 47Ω, ϵ_{re}= 6.8 in the MS case.

Because of the incertainties in the fabrication process, and the slight frequency dependence of the characteristics in the frequency range of 0.5 - 10 GHz, these initially calculated values can be accepted.

B.6 CALCULATED Epsilam-10 DEVICE DIMENSIONS AND CHARACTERISTICS

For the devices on Epsilam-10 substrates, the fixed dimensions are:

h = 1.27 mm
t = 35 μm
and ϵ_r= 10

On Epsilam-10 a lot of microstrip lines, with gaps and continuous lines, are realized. The central stripwidth W is simulated as W = 1.18 mm. This is done with the simulation software "Lignefen" available at LEMO. As an example the results of this simulation are given below. With the equations given in this Appendix, we obtain:

Z_c= 50.5 Ω, ϵ_{re}= 6.8 for the microstrip devices on Epsilam-10 substrates.

```
Microstrip Single Line Synthesis
Z0 =    50.0
H  =     1.270MM      ER =  10.20    TAND =  .00000    T/H =  .0000
Freq =          .5GHZ

W =    1.185MM       Keff =    6.7927


Microstrip Single Line Synthesis
Z0 =    50.0
H  =     1.270MM      ER =  10.20    TAND =  .00000    T/H =  .0000
Freq =          1.5GHZ

W =    1.185MM       Keff =    6.8652


Microstrip Single Line Synthesis
Z0 =    50.0
H  =     1.270MM      ER =  10.20    TAND =  .00000    T/H =  .0000
Freq =          3.0GHZ

W =    1.185MM       Keff =    6.9797
TRL >


Microstrip Single Line Synthesis
Z0 =    50.0
H  =     1.270MM      ER =  10.20    TAND =  .00000    T/H =  .0000
Freq =         10.0GHZ

W =    1.185MM       Keff =    7.6457
```

Figure B.1: SuperCompact Line Synthesis Simulations

The simulation show the weak frequency dependence of the characteristics, as the frequency increases.The dispersion frequency as given in eq.A.3 is calculated as: f_d = 31.3 GHz (with Z_c= 50Ω, and h = 0.635 mm). Below this frequency the dispersion can be neglected.

APPENDIX C

SuperCompact Simulation Files

This Appendix contains the two SuperCompact simulation files used to simulate and optimize the realized devices. In the file Sgap.ckt this is done using the physical dimensions of the (gap-) devices. In the file Circgap.ckt this is done by the equivalent π-circuit of capacitances. The different sections (FREQ, OUT, OPT etc.) as described in Chapter 5, paragraph 5.5 can be seen.

```
SUPER-COMPACT PC V4.06  13-MAR-92  10:54:03  File: sgap.ckt

*SGAP
G1: .2MM
X1: 1.18MM
L1: 0MM

LAD
TRL 1 2 W=X1 P=L1 SUB
GAP 2 3 W=X1 P=G1 SUB
TRL 3 4 W=X1 P=L1 SUB
SGAP: 2POR 1 4
END

FREQ
STEP 0.5GHZ 2.25GHZ 0.1GHZ
END

OUT
PRI SGAP S
PLO SGAP S
END

OPT
SGAP
F=2GHZ 10GHZ MS11=-1DB GT
*F=8.5GHZ 9.75GHZ MS21=-10DB GT
END

DATA
SUB: MS H=1.27MM ER=10.2 MET1=CU 35UM
END.
```

Figure C.1: File Sgap.ckt

```
SUPER-COMPACT PC V4.06  12-MAR-92  18:46:59  File: circgap.ckt

*CIRCGAP
C1: ? .07692PF ?
C2: ? .05572PF ?
*W1: 1.181MM
*L1: 14.9MM
*P1: 14.9MM
*LT1: ? 600NH ?
*CT1: ? 200PF ?
*C0: 299792458.1

LAD
*CAB 1 2 Z=50 P=P1 V=(1/(SQRT(LT1*CT1)*C0))
*TRL 1 2 W=W1 P=P1 SUB
CAP 1 C=C2
CAP 1 2 C=C1
CAP 2 C=C2
*CAB 3 4 Z=50 P=P1 V=(1/(SQRT(LT1*CT1)*C0))
*TRL 3 4 W=W1 P=L1 SUB
CIRCGAP: 2POR 1 2
END

FREQ
STEP .5GHZ 2.25GHZ .1GHZ
END

OPT
CIRCGAP
F=.5GHZ MS21=-32DB PS21=89DEG
F=1GHZ MS21=-26DB LT PS21=86DEG
F=1.5GHZ MS21=-22.5DB LT PS21=83DEG
F=2GHZ MS21=-20DB LT PS21=80DEG
F=2.25GHZ MS21=-19.7DB LT PS21=79DEG
END

*DATA
*SUB: MS H=1.27MM ER=10.2 MET1=CU 35UM
*END.
```

Figure C.2: File Circgap.ckt

APPENDIX D

Equivalent Gap Circuit Capacitances Calculations

The closed form expressions to calculate the capacitances in the equivalent gap circuit can be found in [9]. The equations are found by curve fitting the numerical results given in [21]. The results in [21] are obtained by first excitating the gap discontinuity symmetrically (V volts on port 1 and on port 2) resulting in C_{even}, and afterwards excitating the "two port" anti-symmetrically (V volts on port 1 and -V volts on port 2) resulting in C_{odd}. C_s and C_p are related to C_{even} and C_{odd} by:

$$C_p = \frac{1}{2} C_{even}$$

$$C_g = \frac{1}{2} (C_{odd} - \frac{1}{2} C_{even}) \qquad \text{(D.1)}$$

$$\frac{C_{odd}}{W} (pF/m) = (\frac{l_g}{W})^{m_o} \exp k_0 (\frac{\epsilon_r}{9.6})^{0.8}$$

$$\frac{C_{even}}{W} (pF/m) = (\frac{l_g}{W})^{m_e} \exp k_e (\frac{\epsilon_r}{9.6})^{0.9} \qquad \text{(D.2)}$$

The expressions for C_{odd} and C_{even} are valid for:

$2.5 \le \epsilon_r \le 15$ and $0.5 \le W/h \le 2$

$$m_o = \frac{W}{h} (0.619 \, Log\frac{W}{h} - 0.3853) \qquad (0.1 \le \frac{l_g}{W} \le 1)$$

$$k_o = 4.26 - 1.453 \, Log\frac{W}{h} \qquad (0.1 \le \frac{l_g}{W} \le 1)$$

$$m_e = 0.8675, \quad k_e = 2.043 \, (\frac{W}{h})^{0.12} \qquad (0.1 \le \frac{l_g}{W} \le 0.3)$$

$$m_e = \frac{1.565}{(\frac{W}{h})^{0.16}} - 1, \quad k_e = 1.97 - \frac{0.03}{\frac{W}{h}} \qquad (0.3 \le \frac{l_g}{W} \le 1)$$

These expressions are accurate to within 7%.

The gap-device on the Epsilam-10 substrate has the following characteristics:

l_g = 0.2 mm
W = 1.18 mm ===> $0.1 < l_g/W = 0.17 < 0.3$
h = 1.27 mm
ϵ_r = 10

This results in: m_o = -0.38 k_o = 4.3
m_e = 0.8675 k_e = 2.03

C_{odd} = 0.176 pF
C_{even} = 0.02 pF

C_p = 0.01 pF
C_g = 0.087 pF